Impact of the modulated annual cycle and intraseasonal oscillation on daily-to-interannual rainfall variability across monsoonal India

Vincent Moron (+,*), Andrew W. Robertson (*), Michael Ghil (++, **)
(+) Aix-Marseille Univ, CEREGE UMR 6635, 13545 Aix en Provence cedex 4, France,
and Institut Universitaire de France, Paris, France
(*) International Research Institute for Climate and Society (IRI),
The Earth Institute, Columbia University, Palisades, NY, USA
(++) Department of Atmospheric & Oceanic Sciences and Institute of Geophysics & Planetary Physics,
University of California, Los Angeles, CA 90095-1565, USA
(**) Geosciences Department and Laboratoire de Météorologie Dynamique
(CNRS and IPSL), Ecole Normale Supérieure, Paris, France

September, 23rd 2011

Revised version

Climate Dynamics, sub judice

Abstract

Variability of the Indian summer monsoon is decomposed into an interannually modulated annual cycle (MAC) and a northward-propagating, intraseasonal (30–60-day) oscillation (ISO). To achieve this decomposition, we apply multichannel singular spectrum analysis (M-SSA) simultaneously to unfiltered daily fields of observed outgoing long-wave radiation (OLR) and to reanalyzed 925-hPa winds over the Indian region, from 1975 to 2008. The MAC is essentially given by the year-to-year changes in the annual and semi-annual components; it displays a slow northward migration of OLR anomalies coupled with an alternation between the northeast winter and southwest summer monsoons. The impact of these oscillatory modes on rainfall is then analyzed using a 1-degree gridded daily data set, focusing on Monsoonal India (north of 17°N and west of 90°E) during the months of June to September. Daily rainfall variability is partitioned into three states using a Hidden Markov Model. Two of these states are shown to agree well with previous classifications of "active" and "break" phases of the monsoon, while the third state exhibits a dipolar east-west pattern with abundant rainfall east of about 77°E and low rainfall to the west. Occurrence of the three rainfall states is found to be an asymmetric function of both the MAC and ISO components. On average, monsoon active phases are favored by large positive anomalies of MAC, and breaks by negative ones. ISO impact is decisive when the MAC is near neutral values during the onset and withdrawal phases of the monsoon. Active monsoon spells are found to require a synergy between the MAC and ISO, while the east-west rainfall dipole is less sensitive to interactions between the two. The driest years, defined from spatially averaged June–September rainfall anomalies, are found to be mostly a result of breaks occurring during the onset and withdrawal stages of the monsoon, e.g., mid-June to mid-July, and during September. These breaks are in turn associated with anomalously late MAC onset or early MAC withdrawal, often together with a large-amplitude, negative ISO event. The occurrence of breaks during the core of the monsoon — from late July to late August — is restricted to a few years when MAC was exceptionally weak, such as 1987 or 2002. Wet years are shown to be mostly associated with more frequent active spells and a stronger

MAC than usual, especially at the end of the monsoon season. Taken together, our results suggest that monthly and seasonal precipitation predictability is higher in the early and late stages of the summer monsoon season.

Keywords: Indian monsoon, seasonal rainfall, onset, break, Markov chain, hidden state, singular spectrum analysis.

1. Introduction

Interannual variations of Indian summer monsoon rainfall can have disastrous consequences for more than a billion people (Gadgil 2003; Krishna Kumar et al. 2004). Space-time variations in the monsoon rainfall during Indian summer (e.g., June to September, JJAS hereafter; Table 1 provides the list of all acronyms), though, are governed by phenomena and processes on many scales — from cumulonimbus clouds at the local scale to displacements of the inter-tropical convergence zone (ITCZ) and quasi-divergent circulations at planetary scale (e.g., Meehl 1987; Webster and Yang 1992; Webster et al. 1998; Annamalai et al. 1999; Sperber et al. 2000; Wang and LinHo 2002; Gadgil 2003; Goswami et al. 2003; Goswami 2005; Chang et al. 2005; Preethi et al. 2010). Thus, interannual variability of spatially averaged JJAS rainfall, often calculated in terms of the All-India Rainfall Index (AIRI; e.g., Mooley and Parthasarathy 1984; Parthasarathy et al. 1993, 1995), is relatively small (less than < 10%), but this index hides large regional variations within India that tend to cancel in the sub-continental average (e.g., Webster et al. 1998). Indeed, for the 1-degree rainfall data set described below in Sect. 2.1, the coefficient of variation of JJAS seasonal amounts varies locally between 16% in wetter parts of India (Bengal and the western Ghats) to 145% in the drier ones (Thar Desert), while the spatial mean (median) equals 35% (29%) across the monsoon zone of India, as defined following Gadgil (2003).

The seasonal predictability of Indian summer monsoon rainfall is notoriously poor, operationally (Goddard et al. 2003) as well as in studies of hindcast performance of statistical forecast models (Krishna Kumar et al. 1995; Prasad and Singh 1996) and of general circulation models (GCMs; Gadgil and Sajani 1998; Brankovic and Palmer 2000; Joseph et al. 2010). Large-scale atmospheric indices such as horizontal or vertical shear in the zonal wind have been shown to be more seasonally predictable (Webster and Yang 1992; Goswami and Ajaya Mohan 2001; Mitra et al. 2005; Pattanaik and Kumar 2010), but this better predictability of the large-scale circulation does not necessarily translate to improvements in precipitation predictions over India.

This limited skill in seasonal rainfall predictions has been partly attributed to the large amplitude of intraseasonal variability (ISV hereafter; Waliser et al. 2003). Pioneering work during the 1970s and early 1980s (Murakami 1976; Krishnamurti and Balme 1976; Yasunari 1979, 1980, 1981; Sikka and Gadgil 1980; Murakami and Nakazawa 1985; Lau and Chan 1986) isolated ISV from short records of low-level winds, cloudiness or both, often for a single summer season (Table 2). These studies identified two main oscillations, which organize the space-time variation of monsoon depressions and associated rainfall events and have slightly different periods. The one with the longer period, of 30–60 days, is often referred to simply as the intraseasonal oscillation or northward-propagating intraseasonal oscillation (Klingaman et al. 2008); the second one has an approximate periods of 10–25 days, and is usually referred to as the quasi-biweekly mode (QBM hereafter). In the following, we use the term intraseasonal oscillation (ISO) to refer in general to the whole sub-seasonal period range, including both oscillations.

The characteristics of both oscillations and their impact on Indian rainfall have been the subject of many previous studies, as summarized in Table 2. The QBM is characterized by a largely westward-propagating mode that originates over the northwest tropical Pacific and propagates toward northwest India, passing over the Bay of Bengal (Murakami 1980; Krishnamurti et al. 1981; Chen and Chen 1983; Annamalai and Slingo 2001; Walliser et al. 2003; Chatterjee and Goswami 2004; Hoyos and Webster 2007; Fujinami et al. 2011). The 30–60-day mode, on the other hand, originates in the equatorial Indian Ocean, is related to the Madden-Julian Oscillation (MJO hereafter; Krishnan and Venkatesan 1996; Wang and Xu 1997; Wang and Xie 1997; Kang et al. 1999; Sperber et al. 2000; Slingo and Annamalai 2000; Annamalai and Slingo 2001; Lawrence and Webster 2001, 2002; Vecchi and Harrison 2002; Jian et al. 2003; Sanjeeva and Rao 2005; Hoyos and Webster 2007; Sperber and Annamalai 2008; Ajaya Mohan et al. 2010; Yoo et al. 2010), and it propagates northward. The active phase of the 30–60-day oscillation shows a clear north-south dipole in outgoing long-wave

radiation (OLR) between negative anomalies over India and positive ones over the equatorial Indian Ocean. It also exhibits negative OLR anomalies that extend over the South China Sea to the northwestern Tropical Pacific, while suppressed convection is seen over the northern China Sea and north of the Philippines, thus forming a quadrupole structure (Annamalai and Slingo 2001; Sengupta et al. 2001; Ajaya Mohan and Goswami 2007; Hoyos and Webster 2007; Krishnamurthy and Shukla 2008; Yoo et al. 2010). The north-south dipole structure of the ISO at Indian longitudes has also been interpreted as a fluctuation of the Tropical Convergence Zone between two preferred locations: an oceanic location close to the equator and a continental one over the Indo-Gangetic plain. The northward propagation acts to move the rainfall maximum between these two preferred latitudinal locations (Ajaya Mohan and Goswami 2000; Gadgil 2003).

The impact of the ISO on seasonal rainfall totals is still controversial. The spatial structures of interannual and intraseasonal variability have been shown to be similar (Fennessy et al. 1994; Ferranti et al. 1997; Goswami et al. 1998; Goswami and Ajaya Mohan 2001), which makes their separation difficult. The total duration of monsoon breaks is generally greater for dry years (e.g. 1972) than for normal or wet years; see reviews in Gadgil (2003) and Goswami (2005). Ajaya Mohan and Goswami (2000) found that strong monsoon years are characterized by a higher frequency of active conditions associated with the 30–60 day oscillation, and vice versa. Sperber et al. (2000) also found that strong monsoons are associated with higher probability of occurrence of active conditions, with extended periods of above-normal rain, while the opposite holds for weak monsoons.

Lastly, Qi et al. (2009) noted a negative correlation of $r = -0.59$ between the seasonal variance of the 30–60-day OLR oscillation, spatially averaged over 10°–20°N and 75°–90°E, on the one hand, and the AIRI, on the other. Contrary to the above findings, however, Krishnamurthy and Shukla (2000, 2007, 2008) have concluded that the spatio-temporal structure of rainfall exhibits an intraseasonal meridional tripole structure that is distinct from that in OLR, with its seasonal in-phase

variation throughout India, and that the ISO contributes very little to seasonal rainfall totals. If the ISO were to consist of non-interacting sinusoidal oscillations, there could be no rectified impact of the ISO on the seasonal average. Nonlinearities, however, could lead to a non-zero seasonal residual (e.g., Goswami 2005), as pointed out, in a more general context, by Ghil and Robertson (2002).

The previous studies in Table 2 have almost always employed a temporal pre-filtering of daily data, often using a 3-day or 5-day running mean or band-pass recursive filters, except in Klingaman et al. (2008), who extracted the 30–60 mode from a single large-scale index applied to unfiltered daily OLR data. Subtraction of the long-term mean annual cycle, often computed on a daily basis, is also typical of these studies. This procedure assumes that there is a fixed annual cycle, with variability on intraseasonal and interannual time scales expressed as deviations from it, according to the standard way that seasonal anomalies are defined in studies of climate variability. Still, the presence of a strong seasonal cycle that characterizes the Indian summer monsoon leads us to question the appropriateness of such a framework. Wu et al. (2008) have proposed an alternative reference frame consisting of an annual cycle that is modulated in its phase and amplitude, with interannual variability expressed in terms of these modulations, with respect to a fixed annual cycle.

The purpose of this paper is to revisit the question of intraseasonal-to-interannual variability of the Indian summer monsoon, using a framework that allows the ISO and interannual modulations of the monsoon's seasonal cycle to be treated in a unified oscillatory way, and without the need for explicit pre-filtering of the data in the time or frequency domain. A multi-channel singular spectrum analysis (M-SSA) is applied to the leading principal components (PCs) of the unfiltered daily OLR and low-level winds; this acts as a data-adaptive filter that focuses attention on the main regional-scale standing and propagating oscillations, while eliminating local-scale and/or stochastic "fast" variability. This approach is used to interpret large-scale monsoonal circulation variability as a combination of a modulated annual cycle (MAC) and the ISO. The impact of these oscillatory compo-

nents on rainfall is then investigated using a simple three-state description of daily rainfall over the core monsoon zone, by using a hidden Markov model (HMM).

The paper proceeds as follows. Section 2 describes the data sets and statistical methods used. The results appear in Sects. 3 and 4, with the large-scale oscillatory behavior described in Sect. 3, while the HMM for the local rainfall and the connection of its states with the oscillations of Sect. 3 are presented in Sect. 4. Concluding remarks follow in Sect. 5.

2. Data and methods

2.1 Observed data sets

The analysis is based on daily interpolated OLR data from the U.S. National Oceanic and Atmospheric Administration (NOAA) on a 2.5-degree latitude-longitude grid, derived from twice daily AVHRR soundings (Liebmann et al. 1996). The data set was obtained over the 34-year span from 1 January 1975 to 31 December 2008 over the domain (60°–100°E, 0–35°N), **(**http://www.esrl.noaa.gov/psd/data/gridded/data.interp_OLR.html**)**. The missing values between 17 March and 31 December 1978, due to satellite failure, were replaced by the daily mean computed from the other years.

Daily wind data were obtained from the NCEP/NCAR reanalysis data set (Kalnay et al. 1996) at 925 hPa, with the same domain and spatial grid as the OLR data set, through the IRI/LDEO Climate Data Library (http://iridl.ldeo.columbia.edu/).

Daily gridded 1-degree rainfall data were prepared by Rajeevan et al. (2005, 2006) from 1803 stations, and were provided by the Indian Meteorological Department for the 1971–2008 period. Note that the resulting 357 grid boxes filter out rainfall variability at spatial scales below about 100 km.

2.2 Multichannel singular spectrum analysis (M-SSA)

M-SSA is an extension of the classical empirical orthogonal function (EOF) analysis to a delay-coordinate phase space; see Ghil et al. (2002) and references therein. It is a data-adaptive spectral method, in which the bandwith and shape of the filters are provided by the data instead of the user. M-SSA consists of diagonalizing the lag-covariance matrix of the multi-channel time series with lags ranging from 0 to M–1. The window width is $W = M\delta t$, with δt = 1 day being the sampling interval. We chose M = 60 to capture the ISO, and applied M-SSA to unfiltered OLR, together with the zonal and meridional components of the wind at 925 hPa.

The variables were standardized first to zero mean and unit variance, and weighted by the squared cosine of latitude. A standard EOF analysis was applied to this data set to extract the 22 leading principal components (PCs); these 22 PCs account for 75% of the total variance and were then used as the 22 “channels” in the M-SSA. M-SSA allows the identification of robust oscillations, with periods between roughly W and W/3 (Ghil et al. 2002). The oscillations are identified as pairs of eigenfunctions with similar eigenvalues and associated space-time EOFs (ST-EOFs) and temporal PCs (ST-PCs) that are in phase quadrature; such a pair represents therewith a data-adaptive sine-cosine pair for a given oscillation. In this analysis, we do not identify components whose period is greater than W as pairs, even if they represent oscillations.

Note that increasing the window width to 365 days allows the annual and semi-annual cycles to be identified as pairs of eigenmodes, but the main ISO components (period < 80 days) are not well resolved with such a wide window. Window widths of 80 or 120 days lead to very similar results to those presented in the following (not shown). Very similar ISO components are also obtained when the M-SSA is carried out in two steps with two distinct window widths, first identifying the annual and semi-annual cycles, and then applying M-SSA a second time to the time series with these components removed. The use of a one-tiered M-SSA with single window width of 60 days is able to

adequately resolve the annual cycle despite its longer period; this ability is due to the large number of annual samples in the dataset, and has the advantage of simplifying the analysis.

Reconstructed components (RCs) have been computed using the method of Plaut and Vautard (1994). The RCs are filtered versions of the original sequences of maps, obtained by projecting the raw data onto subsets of ST-EOFs. The RCs are estimated first in the EOF space using ST-EOFs and ST-PCs, as in Vautard et al. (1992). The resulting 22 RCs are then post-multiplied by the 22 leading EOFs to recover their space-time patterns in physical space. The RCs are equal in length to the original signal and retaining the whole set of ST-EOFs allows one to recover the complete original fields. Thus, the RCs isolate the slowly changing phase and amplitude of a given oscillation.

2.3 Phase compositing

RCs 1–4 capture the MAC, while RCs 5–6 represent the ISO: see Sects. 3.1 and 3.2. To obtain phase composites of these oscillations, OLR grid point fields were interpolated first linearly to a 1°x1° grid and then averaged spatially over the core monsoon region of northern India (17°N–30°N, 66°E–89°E), following Gadgil (2003, Fig. 4a). The resulting time series $x(t)$ of MAC and $y(t)$ of the ISO, and their time derivatives $x'(t)$ and $y'(t)$, respectively, were then normalized. The time series within each pair ($x(t)$, $x'(t)$) and ($y(t)$, $y'(t)$), respectively, are by definition in approximate phase quadrature. The phase and amplitude can, therefore, be defined by the argument and the modulus of the complex number $x'(t) + ix(t)$ for the MAC, and of $y'(t) + iy(t)$ for the ISO. Doing so provides a practical way to define objectively the instantaneous state of the oscillations (Moron et al. 1998; Ghil et al. 2002). The MAC and ISO components in OLR and in the zonal and meridional wind components, u and v, were then averaged according to their instantaneous phase to construct composites.

2.4 Hidden Markov Model (HMM)

An HMM is used to obtain a parsimonious, discrete, state-based description of rainfall variability from the 1-degree daily gridded rainfall data, in order to capture the larger-scale active and break phases in rainfall, while filtering out synoptic and smaller scales of rainfall variability. The HMM used here follows the approach of Hughes and Guttorp (1994) to model daily rainfall occurrence, while additionally modeling rainfall amounts; it is fully described in Robertson et al. (2004, 2006), and has been applied to Indian rainfall by Greene et al. (2008, 2011). In brief, we assume that the time sequence of daily rainfall measurements on a network of stations is generated by a first-order Markov chain of a few discrete hidden (e.g., unobserved) rainfall "states." For each state, the daily rainfall amount at each station is modeled as a finite mixture of components, consisting of a delta function at zero amount to model dry days, and a combination of two exponentials to describe rainfall amounts on days with nonzero rainfall. The homogeneous version of the HMM is used here, in which the state-transition matrix is treated as being constant in time. The HMM is applied to all 1-degree grid points within Monsoonal India.

We performed parameter estimation using the maximum likelihood approach, via the iterative expectation-maximization (EM) algorithm (Dempster et al. 1977; Ghahramani 2001). The algorithm was initialized 10 times from random starting points, the run utilized being that with the highest log-likelihood. Estimation was performed using the Multivariate Nonhomogeneous Hidden Markov Model Toolbox (S. Kirshner, http://www.stat.purdue.edu/~skirshne/MVNHMM/).

3. Intraseasonal and interannual oscillations

3.1 Spectral analysis of OLR and wind data

Results from applying M-SSA to the combined fields of year-round daily OLR and 925-hPa winds in the large-scale region (60°–100°E, 0–35°N) are shown in Fig. 1, in terms of the power spectra of ST-PCs 1–10. The power spectra shown in Fig. 1 were computed by applying the maximum entropy method to each ST-PC separately. The four leading modes (Fig. 1) — which are dominated by the

annual and semi-annual harmonics — largely account for the variability with periods longer than the window width of 60 days. These four components capture 55% of the variance, in the conventional EOF–pre-filtered data; their sum is referred to hereafter as the “modulated annual cycle” (MAC), because their phase and amplitude are modulated from year to year (Wu et al. 2008).

The first resolved oscillatory pair is given by modes 5–6, which exhibit a broad spectral peak near 40 days, and capture 2.5% of the variance; it is this pair that is referred to hereafter as the ISO. By construction, the MAC and ISO are linearly independent. The following modes each capture less than 1% of the variance and are not discussed further. The QBM found in previous studies (Hoyos and Webster 2007; Krishnamurthy and Shukla 2008; Fujinami et al. 2011) that used temporally pre-filtered data does not appear as a statistically significant component. When redoing the M-SSA with a shorter, 40-day window or by subtracting the MAC RCs first, the results (not shown) are quite similar.

The MAC accounts for 40–60% of the total year-round OLR variance across India, but decreases to less than 10–15% within the summer season, while the ISO captures about 1–15%, with a slight seasonal increase during the summer, and with a spatially northward decrease from a near-equator maximum (not shown). The ratio of variance accounted for by the ISO compared to the MAC RCs within JJAS decreases northward, as shown in Fig. 2a, from greater than unity over southern India to very small values over northern India. The seasonality of the ISO amplitude is shown in Fig. 2b in terms of the zonal average (60°–100°E) of the daily standard deviation of ISO OLR. The short--wave pattern in time in this panel is just an effect of the shortness of the available record. The ISO is pronounced over the Indian Ocean from May to November, and much weaker during the boreal winter. Its highest amplitude coincides with the onset of the monsoon in May–June, with a secondary peak near its withdrawal at the end of September and in early October.

3.2 Reconstruction of the MAC and ISO patterns

Reconstructions of the zonally averaged OLR associated with the MAC and ISO are illustrated in Fig. 3 for the year 1987. The seasonal variation is clearly isolated by the MAC (Fig. 3b), together with the striking temporal asymmetry of the abrupt onset and smoother retreat of the summer monsoon (Chang et al. 2005). The ISO (Fig. 3c) is active from May to December (see also Fig. 2b), with a clear northward propagation that is visible even in the raw data (Fig. 3a). For example, two spells of positive OLR anomalies, indicating suppressed deep convection, propagate northward from the equator around early July and late August (Slingo and Annamalai 2000; Lawrence and Webster 2001). Another ISO pulse is almost synchronous with the large-scale onset of the monsoon in late May (Fig. 3a,c). The ISO amplitude is larger at the equator and almost vanishes north of 20°–25°N (Fig. 3c) as seen in Fig. 2. Vernekar et al. (1993) and Lawrence and Webster (2001) already indicated that the MJO had larger amplitudes in 1987 than in 1988.

The spatio-temporal structures of the MAC and ISO are shown in Figs. 4 and 5, respectively, by using composites that divide each cycle into eight phase categories, as described in Sect. 2.3 (Moron et al. 1998; Ghil et al. 2002), and plotting the OLR and wind fields as standardized anomalies. The MAC phases (Fig. 4) are ordered according to their annual cycle, while the “fixed” calendar dates for the phase composites reflect the averaging of the composites across years (i.e. each phase occur 50-100% of years during the time windows noted in Fig. 4). Due to the rather strong semi-annual component of OLR, the winter phases 1 and 3 occur both before and after the summer monsoon season (Figs. 4a,c), when clear skies produce hot surface temperatures that give rise to two pronounced OLR maxima across Peninsular India.

The MAC exhibits a predominantly standing-wave, north-south pattern, with little spatial phase propagation, as seen already in Fig. 3b. The “winter” regime is most pronounced in phases 1 (Fig. 4a) and 2 (Fig. 4b) with positive OLR anomalies across peninsular India and the adjacent areas of

the Arabian Sea and the Bay of Bengal, accompanied by E–NE wind anomalies, while negative OLR anomalies associated with colder surfaces, high clouds or both accompanying extratropical disturbances are seen north of about 30°N. Phase 3 (Fig. 4c) is a transition toward the summer regime with an anomalous cyclonic circulation visible over the Arabian Sea. The summertime regime is exemplified by phases 4–6 (Figs. 4d–f), with negative OLR anomalies across India and positive ones over the deserts to the north as well as over the Tibetan Plateau. Southwesterly-to-westerly wind anomalies cover most of the domain with an anomalous closed cyclonic center over southern Pakistan and a trough across northern India. Phase 7 represents the transition toward the winter regime with an anomalous closed cyclonic circulation centered over the northeast coast of India (Fig. 4g) and a clear decrease in amplitude of the negative OLR anomalies across India.

The phase composites of the ISO (Fig. 5) are characterized by a northward propagation of OLR anomalies, with a strongly reduced amplitude north of about 20°N, in agreement with previous studies (see Table 2). Elliptical anomalies appear near the equator, southeast of Sri Lanka; they tend to split on either side of peninsular India as they propagate northward and form two separate centers of action over the Arabian Sea and Bay of Bengal that are associated with well-defined cyclonic wind anomalies in the negative phase (Figs. 5b,c), while positive OLR anomalies already appear south of 10°–15°N (Figs. 5b,c). In phase 4, the western cyclonic circulation anomaly center weakens close to the seasonal heat low over southern Pakistan during summer (Figs. 4d–g), while the eastern one remains strong over the northern Bay of Bengal, and thus favors monsoon depressions there (Goswami et al. 2003). The wind anomalies in phase 3 imply low-level convergence over central India (Fig. 5c), and over northeastern India in phase 4 (Fig. 5d). The positive OLR anomalies associated with anticyclonic anomalies across monsoonal India propagate northward during phases 5–7, while negative OLR anomalies appear close to the equator in phase 7 (Figs. 5e–g).

3.3 Relationships with spatially averaged daily rainfall

Figure 6 shows MAC and ISO components of OLR standardized anomalies, together with daily rainfall averaged across Monsoonal India, defined as the region north of 17°N and west of 90°E (Gadgil 2003), for two dry years (left column) and two wet years (right column). Note that the MAC and ISO spatial averages are multiplied by -1 so that positive values correspond to positive rainfall anomalies and ISO curves (in red) have been multiplied by a factor of three for clarity. The annual and semi-annual harmonics are both clearly present in the MAC, and regional-scale rainfall onset appears closely linked to the sharply decreasing tendency of MAC around early June.

The relationship with rainfall cessation in September is not as clear, as rainfall tends to persist in October in 2002 (Fig. 6c) and 2003 (Fig. 6d), or even in November in 1987 (Fig. 6a). Both dry years are characterized by breaks and active phases during the monsoon season when daily mean intensity can be nearly as large as during the wet years. The breaks in 1987 (Krishnamurti et al. 1989) and 2002 (Kripilani et al. 2004; Bhat 2006; Saith and Slingo 2006; Sajani et al. 2007) appear to be the consequence of a weaker than usual MAC, especially in 1987 (Fig. 6a), coupled with negative ISO episodes, corresponding roughly to ISO phases 6-7 (Fig. 5f,g) (Vernekar et al. 1993; Lawrence and Webster 2001). Similar negative ISO episodes also occur also during the wet years, but they are accompanied by a MAC that is stronger than usual, and rainfall is almost continuous, in the large-region average. The amplitude of the ISO is also weaker during the wet JJAS season of 2003 (Fig. 6d).

4. Daily rainfall and its relationship to ISO and MAC

4.1 Hidden Markov model of daily rainfall

The HMM decomposition of daily rainfall variability into three discrete states is shown in Fig. 7, in terms of the probability of rainfall (left column, panels a–c), and the mean rainfall intensity on wet days (right column, panels d–f), for each of the states. The three-state model provides a coarse-grain discretization that captures the large-scale aspects of seasonality, active and break phases, and spa-

tial contrasts; similar results were found using a 4-state decomposition in Greene et al. (2011). Rainfall in state 1 is characterized by an east-west dipolar pattern (Gadgil 2003) with high rainfall probabilities, and large mean rainfall amounts on wet days in the east and on the west coast near 18°N, with dry conditions elsewhere (Figs. 7a,d). State 2 is wet almost everywhere, especially south of about 24°N, with relatively drier conditions further north (Figs. 7b,e). State 3 is dry almost everywhere, except in the northeast corner of the domain, near Assam (Figs. 7c,f).

Very similar results to those presented below were found using NHMMs with 3-10 states with the spatial average of rainfall, on a daily time scale, as a predictor to test the predictability from a "perfect" spatial average (not shown). As usual in this statistical-model context, the advantage of 3 states over a larger number was usually small, but 3 had also the advantage of Occam's razor: the simpler the better. Thus, the choice of 3 states was further justified by the fact that it was the minimal number required to consider properly the wet phases and breaks, since Gadgil (2003), Gadgil and Joseph (2003) and Rajeevan et al. (2008) amongst others often distinguish between eastern and western breaks.

In terms of anomaly, state 3 (Figs. 7c,f) is associated with homogeneous negative anomalies, especially for mean rainfall amount, since the weighted spatial average equals –64%, with a single positive-anomaly grid-point. Positive anomalies of rainfall probability clearly dominate state 2 (Fig. 7b), while positive anomalies of mean rainfall amount are almost in phase quadrature between state 2 (Fig. 7e) and state 1 (Fig. 7d), while the spatial average equals +62% for state 2 and 0% for state 1.

Once the parameters of the HMM have been estimated, the most likely daily sequence of states can be determined using a dynamic programming scheme called the Viterbi algorithm (Forney 1978). The Viterbi sequence, which expresses the evolution of rainfall patterns over the entire time series,

in terms of the hidden states, is used to build composites of OLR and wind anomalies for each state, with respect to the JJAS seasonal average in Fig. 8. The dipolar rainfall pattern of state 1 is accompanied by negative OLR anomalies east of 72°E, anomalous southwesterlies over Pakistan, and weak anomalous cyclonic centers near (65°E, 32°N) and (81°E, 25°N); the former center is dry and suggests a heat low (Fig. 8a). The wet state 2 coincides with an intensified southwest monsoon flow that exhibits a strong anomalous cyclonic center near (70°E, 23°N) and a trough axis extending southeastward to the Bay of Bengal (Fig. 8b). The dry state 3 is associated with broad-scale positive OLR anomalies centered over northwest India, anomalous anticyclonic vorticity, and a weakened monsoon flow, with respect to the seasonal average (Fig. 8c).

A large degree of seasonality is reflected in the HMM rainfall states and their accompanying circulation anomalies. This is seen clearly in the estimated Viterbi sequence, which is shown in Fig. 9. State 3 (yellow squares in the figure) is naturally more prevalent in June and September, before and after the core of the monsoon, but also occurs in short spells during July–August in some years (e.g. in 1987, 1993, and 2002). States 1 (green squares) and 2 (blue squares) are concentrated in July–August without any clear temporal preference. Following Greene et al. (2008), we compared the state sequence with published chronologies of active and break periods. Gadgil and Joseph (2003) compared various definitions of monsoon breaks and found substantial differences among them, although the interannual variability of the number of break days resulting from these definitions is more consistent. Rajeevan et al. (2008) has constructed chronologies of both active and break days for the period July–August 1975–2007, and these are shown superimposed on the HMM state sequence in Fig. 9 as black and red dots, respectively. The 252 break days fall mostly into State 1 (82 days) and state 3 (160 days), with the remaining 10 classified as State 2.

The relatively large fraction (about 33%) of break days assigned to State 1 is consistent with Gadgil and Joseph (2003), who found many breaks confined to northwest India. The 239 active days fall

largely into State 2 (195 days) and to some extent into State 1 (44 days). The HMM classification thus captures the broad distinctions between active (> 80% in State 2) vs. break (> 95% in States 1 or 3) spells of the monsoon and has the advantage of providing a continuous record of all days, whereas only 24% of July–August days were classified by Rajeevan et al. (2008). The state sequence also casts the break days during the peak of the monsoon in the context of the dryer periods on either side (Fig. 9).

Interannual variability of spatially averaged JJAS rainfall anomalies across Monsoonal India is strongly correlated with the frequencies of occurrence for State 2 (r = 0.83***) and State 3 (r = –0.87***), but not with State 1 (r = 0.19). In the following, one, two, and three asterisks indicate correlations that are significant at the 90, 95, and 99% two-sided level according to a random-phase test (Janicot et al. 1996). These correlation values were computed from standardized rainfall, where values at each grid point from Monsoonal India were normalized by its interannual standard deviation, prior to making the spatial average, thus defining a standardized anomaly index (SAI). Note that using the more common AIRI, as defined in Sect. 1, leads to very similar results, since the correlation between the AIRI and the SAI for Monsoonal India, as defined here, equals 0.99***. The low correlation value for State 1 is consistent with the dipolar pattern of rainfall in this state (Fig. 7a), since the SAI consists of a spatial averaging of anomalies.

4.2 Relationships between oscillatory components and rainfall states

To analyze the relationships between the occurrence of the three rainfall states, on the one hand, and the MAC and ISO oscillatory modes of OLR and circulation, on the other, we use the spatial-average indices of the MAC and ISO constructed in Sect 2.3 from the OLR RCs over the Monsoonal India region. The indices are then standardized to zero mean and unit variance over all 34 JJAS seasons from 1975 to 2008.

The dependence of rainfall-state occurrence on the MAC and ISO indices is shown in Fig. 10, with the polarities of these OLR indices reversed as in Fig. 6, such that the positive phases of each index (i.e., the negative OLR anomalies) coincide with positive rainfall anomalies. Each panel of Fig. 10 shows the frequency of the rainfall state expressed as a conditional probability, given the amplitude of both MAC and ISO indices. The marginal distributions as a function of each index alone are given in the top row (for ISO) and the right column (for MAC) of each panel. For each cell in Fig. 10, the sum over the three states is equal to one. All the probabilities were tested using a Monte Carlo scheme in which the chronology of states was reshuffled 1000 times and the probabilities were recomputed with the indices left untouched. The significance level of the observed probabilities was then estimated from the ranked distribution of the 1000 random probabilities and only the values significant at the two-sided 90% level are displayed in Fig. 10.

The occurrence of the dry State 3 (Fig. 10c) is largely controlled by MAC, with 51% of days assigned to this state occurring when MAC < –1 (which corresponds to 19.7% of all days studied), and only 8% of State-3 days occurring when MAC > 0.5 (40.4% of all days). The impact of ISO on State 3 is weak for these MAC categories, but becomes significant when MAC is between –1 and 0.5, with positive ISO favoring fewer State-3 occurrences. This behavior is consistent with the strong seasonality of MAC, together with the high prevalence of State 3 at the beginning and the end of the monsoon season (Fig. 9). It also indicates, however, that ISO has an important impact on rainfall during the onset and withdrawal stages of the monsoon, when ISO itself reaches its largest amplitude (Fig. 2b). Neutral MAC values between –1 and 0.5 occur in over 50% of years between June 13 and July 3, and between August 24 and September 18; such neutral MAC values occurred only in 1987 and 2002 during the core of the season (July 17–August 14). Thus, the occurrence of large-scale monsoon breaks (State 3) is very limited from mid-July to mid-August, except when MAC is exceptionally weak, and its occurrence, outside the normally dry periods before and after the boreal-summer monsoon depends upon being favored by both MAC and ISO values. The im-

pact of ISO on State 3 is especially important for MAC values between 0 and –0.5 (Fig. 10c), which occurs in over 33% of years in the June 19–25 and September 2–12 periods.

The interaction between MAC and ISO is more substantial for the wet State 2 that coincides with active spells of the monsoon. The marginal MAC and ISO distributions are more similar in this case, and there is a systematic tendency for low State-2 probabilities when MAC and ISO values are negative, and toward high State-2 probabilities when MAC and ISO values are positive (Fig. 10b). Nevertheless, the seasonal cycle still plays a significant role: thus large negative MAC values, of less than –1.5 occur almost exclusively in early June and late September and they are associated with very small wet-state probabilities (Fig. 10b). On the other hand, MAC values that are higher than 0.5 are not sufficient, just by themselves, to get an "active" spell and positive ISO is then required to get a probability larger than 60% (Fig. 10b).

The dependence of State 1, with its west-east dipolar rainfall, on ISO is the least pronounced, which is consistent with the large longitudinal scale of the ISO. State 1 is favored when MAC is positive, e.g., during the core of the summer monsoon, as apparent also from the Viterbi state sequence (Fig. 9). There is some symmetry in the frequency of States 1 and 2 for MAC values above –0.5, e.g., mostly from mid-June to mid-September, with ISO values over 0.5 favoring State 2, especially when MAC is strongly positive, while negative ISO favors State 1. The neutral values of ISO, between –0.5 and 0.5, lead to almost as many occurrences of State 1 as of State 2 (Figs. 10a,b).

The relationship between ISO and rainfall state is further analyzed in Fig. 11 by computing the occurrence probability of each state for days falling within the eight ISO phase categories shown in Fig. 5. The deviation in state probability is defined as observed–expected)/expected and it is plotted along with its statistical significance from a Monte Carlo test of 1000 random permutations of the Viterbi sequence. States 2 and 3 are strongly phase-locked to the ISO, in agreement with the results

in Fig. 10: State 2 is most common during phase 3 (+67%, Fig. 5c) and least common during phase 7 (–50%, Fig. 5g), while the reverse is observed for State 3 (–64% for phase 3 and +54% for phase 7). Thus, active monsoon spells, e.g., State 2, tend to be associated with the twin, northward-propagating, cyclonic anomalies over the Arabian Sea and the Bay of Bengal (Figs. 5b,c). The deviations are weaker for State 1, but nevertheless significant at the two-sided 90% level for phase 2 and from phase 4 to phase 6; the highest positive (negative) anomaly equals +20% (-37%) and occurs for phase 4 (phase 2) (Fig. 5e).

4.3 Interannual variability of the oscillatory modes and rainfall states

We investigated next the interannual variability of the oscillatory modes in terms of their key characteristics, including the onset, withdrawal and mean intensity of the MAC, and the mean amplitude of the ISO. The MAC intensity is computed as the JJAS average, while its phase is computed by comparing each May–October time sequence with its climatological mean, taking the integrated difference over May–June and September–October to define the onset and withdrawal respectively; the anomalous monsoon duration is then taken to be the difference between the two. For the ISO, we evaluate the seasonal mean intensity as the standard deviation of daily values over JJAS. Area-average indices are then defined using the SAI, which is plotted for each index and for the JJAS rainfall amount in Fig. 12.

As expected, the spatial coherence in all of these MAC and ISO indices is high across Monsoonal India, as seen in their interannual variances that are always very close to 1 (see Table 3). This contrasts with seasonal rainfall amounts where the spatial coherence is weak. As found by Moron et al. (2007), the frequency of wet days is more spatially coherent (Table 3) while the SAIs of seasonal amounts and frequencies are correlated at 0.93***. These SAIs are also correlated > 0.95*** with the corresponding leading EOFs (not shown) suggesting that SAI recovers the weak common signal across Monsoonal India.

The MAC onset and withdrawal anomalies are uncorrelated with each other (Table 4 and Fig. 12a) but broadly consistent with the large-scale estimates of Xavier et al. (2007), which were based on inter-hemispheric thermal gradient in the lower troposphere, especially for the onset date, for which the correlation coefficient is r = 0.76***, and somewhat less for the withdrawal date, with r = 0.46**.

The average MAC intensity is by definition related to both the onset and withdrawal dates (Table 4), since a delayed onset, an early withdrawal or both lead to a contracted JJAS curve above 0. Linearly removing the influence of onset and withdrawal dates, however, by using a multivariate regression (light solid line with open circles in Fig. 12b) does not change its temporal behavior greatly. The large deviations in intensity in 1987 and 2002 (weak monsoons) and 1994 (strong monsoon) are especially clear in the residuals. When MAC intensity is computed only during the core of the monsoon (July–August), the correlations with onset and withdrawal drop from –0.62*** and 0.62*** to –0.16 and 0.50***, respectively. Note also that the correlation between the July–August MAC intensity and the residuals of JJAS MAC intensity equals 0.92***. Thus MAC onset is largely independent of both MAC withdrawal and MAC intensity during the core of the monsoon season, while late withdrawal dates do appear to follow large July–August intensities and vice versa.

Interannual variations in MAC onset date are compared to local-scale onset dates in Fig. 13a. We use an “agronomic” definition (Sivakumar 1988; Moron et al. 2009), e.g., the first wet day of a 5-day wet spell that receives at least the mean amount of rainfall of 5-day wet sequences, and is not followed by a 15-day dry spell that receives less than 5 mm in the following 30 days. There are large deviations across Monsoonal India, since the interannual variance of the SAI of the local-scale onset equals 0.10, but the spatial average is consistent with spatial average of MAC onset, with a correlation between the two of r = 0.69***, especially so before about 2000. Figure 13b shows the

frequency of local-scale onset date according to the eight phases of MAC and ISO, spatially averaged across Monsoonal India, computed in the same way as in Sect. 3.2 (Figs. 4 and 5). Local-scale onset occurs, by-and-large, during phase 4 of the MAC, when negative OLR anomalies are still largest over the Arabian Sea and Bay of Bengal (Fig. 4d); it depends also strongly on the ISO phase, as it peaks in ISO phases 1–3, when low-level cyclonic centers form near Kerala and propagate northward on either side of the peninsula (Figs. 5a–c).

4.4 Connection between the oscillatory modes and interannual variations of monsoon rainfall

To investigate the relationship between seasonal amounts, occurrence of the rainfall states and MAC amplitude, we selected the 11 driest and 11 wettest years, e.g., the lower- and upper-tercile categories, from the SAI of JJAS rainfall amount averaged across Monsoonal India (Fig. 12d). Maps of local 1-degree standardized anomalies of JJAS seasonal rainfall amount and rainfall frequency, as well as the occurrence of each HMM state and MAC intensity, are displayed in Fig. 14. The rainfall amount anomalies in the below-normal category (Figs. 14a,c) tend to be more spatially coherent than the wetter-than-normal years (Figs. 14b,d), and anomalies are less significant toward the northeast; the latter is potentially due to the larger role of State 1 there. Rainfall frequency is clearly more spatially coherent than the seasonal amount, which is consistent with the interannual variances of the corresponding SAI shown in Table 2.

The below-normal category of rainfall is associated with higher prevalence of the dry State 3 and less of the wet State 2 from mid-June to early July, and then again in September (Fig. 14e), thus reflecting changes in the length of the monsoon season. The tendency toward more breaks (State 3) during the core of the monsoon season is nonetheless significant; it can be traced, in particular, to the years 1987, 1993, 2000 and 2002 (see again Fig. 9). The wettest 11 years are associated with lower prevalence of the dry State 3, especially from mid-June to early July, and then from August onward, and higher prevalence of the wet State 2 around the end of June, late July, and most promi-

nant from late August onward (Fig. 14f). The prevalence of the State 1 is generally not significantly different between the below-normal and above-normal categories, consistent with its dipolar structure (Fig. 7). Thus, the main significant changes in state frequency occur near the onset and end of the monsoon season, with consistent departures seen in the wet and dry states (States 1 and 3), while broad-scale rainfall anomalies during the core of the monsoon season are less marked in state frequency.

The amplitude of the MAC shows consistent deviations between the two sets of years (Figs. 14g,h), especially from mid-June to late-July and then in September, although the deviations do not always exceed the 95% significance level, as computed from 1000 randomly chosen sets of 11 years each. Thus, the MAC as well as the deviations in state frequency suggests that JJAS seasonal anomalies across Monsoonal India are predominantly due to the changes in the length of the monsoon season.

The within-season modulation of regional-scale rainfall anomalies during the 11 driest and 11 wettest years is further illustrated in Fig. 15 by plotting the SAI values of 10-day averaged rainfall for each category. Significant decadal rainfall anomalies occur mostly in the third decade of June and the first one of July, and again in August and September. This temporal signature is stronger in the below-normal years, and strongest in rainfall frequency (Fig. 15b).

5. Summary and conclusions

We have examined the relationships between large-scale atmospheric oscillations and local-scale rainfall over Monsoonal India — defined here as north of 17°N and west of 90°E — at intraseasonal and interannual time scales. Our approach is based on applying multichannel singular spectrum analysis (M-SSA) simultaneously to unfiltered daily OLR and to the zonal and meridional components of 925-hPa winds from the NCEP/NCAR reanalysis over the region (60°E–100°E, 0°–35°N).

The daily OLR and low-level winds were first projected onto the 22 leading EOF; these 22 EOFs account for 75% of the whole variance and the associated PCs serve as our M-SSA channels. This EOF pre-filtering allowed us to focus on the main regional-scale oscillations without the need for explicit time filtering; it also permitted the identification and characterization of a modulated annual cycle (MAC) that corresponds to the annual and semi-annual cycle, on the one hand, and of the main intraseasonal oscillation (ISO), with a broad peak between 30 and 60 days, on the other. We did not detect a westward quasi-biweekly mode (QBM), as described by Hoyos and Webster (2007) and Krishnamurthy and Shukla (2008) amongst others. Its absence is unlikely to be due to its intermittence or seasonality since the ISO is easily detected, in spite of its sharing both of these properties. Possible reasons may be the smaller spatial scale or reduced amplitude of the QBM over the region considered here.

Our approach to the MAC bears some similarity to Wu et al.'s (2008) the extended empirical mode decomposition study, but M-SSA is capable of extracting the ISO from year-round as well. The ISO is obtained here despite being intermittent, largely absent during winter (Fig. 2b), and its small variance (Figs. 2a, 3). The MAC and ISO are shown to represent the dominant components of atmospheric circulation variability over India (Figs. 4, 5). A new result is the seasonal modulation of ISO, whose amplitude peaks near monsoon onset and withdrawal (Fig. 2b).

The spatially averaged rainfall deficits in the poor monsoons of 1987 or 2002 reflect a weak MAC, while the wet years of 1988 or 2003 are associated with a strong MAC (Figs. 6, 12b). The impact of the ISO is greater during years of weaker MAC, when it can give rise to major breaks (Figs. 6a,c).

The relationships between the MAC and ISO with daily rainfall were quantified using a state-based analysis of gridded rainfall using a hidden Markov model (HMM).

A three-state model consisting of states that are “dry” (State 3), “wet” (State 2), and “wet-in-the-east” (State 1) is found to describe the main attributes of the monsoon rainfall seasonal cycle and active and break phases identified by Gadgil and Joseph (2003) and Rajeevan et al. (2008) in previous studies (Figs. 7, 9). The occurrence of State 3 is associated with anomalously anticyclonic conditions and weakened monsoon flow, while State 2 coincides with an intensified monsoon circulation (Fig. 8). Interannual monsoon rainfall variability over western India is well reproduced by interannual changes in the frequency of occurrence of States 2 and 3, while State 1 is also important over eastern India.

States 2 and 3 are shown to be strongly modulated by the MAC and ISO, with positive MAC and ISO excursions favoring the monsoon’s active phase, and the reverse for the break phase, while, the impact of ISO is stronger for near-neutral values of MAC, particularly near monsoon onset/withdrawal; indeed, local monsoon onsets appear to be triggered just ahead of the northward-propagating ISO (Figs. 10, 13). Although State 1 (“wet-in-the-east”) appears less sensitive to the MAC and ISO, its occurrence is more frequent when the northward-propagating ISO cyclonic anomaly nears the Bay and Bengal during ISO phases 4-5, and thus may follow State 2 that occurs when the anomalous trough lies to the south during ISO phases 2-3 (Fig. 5).

By considering the impacts of the MAC and ISO on rainfall explicitly, these findings augment previous studies in which the impacts of ISO and of interannual monsoon variability were analyzed separately (Table 2); they also make explicit the intraseasonal cyclic transitions seen in the HMM state-transition matrix, found over India by Greene et al. (2008).

The mean seasonal amplitude of the ISO is found to have a weak but finite impact on interannual rainfall variability (Fig. 12 and Table 4). Despite the symmetry, by definition, of the ISO about zero, there is an asymmetry with rainfall that appears to arise due to several factors: (1) nonlinearity in

the impact of the combined MAC+ISO on rainfall, for example, a weak MAC would bolster the role of the “anticyclonic” ISO phase — with more breaks, less active spells or both — vs. the “cyclonic” phase of the ISO; (2) a related seasonal modulation because MAC is weak near monsoon onset/withdrawal, tending to enhance the ISO-related break phases then, and (3) a spatial asymmetry in which the strongest anomalies of JJAS rainfall amounts during dry and wet years are modulated in space, with a stronger signal in the southern and western parts of Monsoonal India (Fig. 14). We need to be cautious here about potential sampling uncertainty, since the analyzed time interval is rather short but the asymmetry could also be due to the actual evolution of ISO itself (Fig. 5).

At local scales on the 1-degree grid of the IMD rainfall data, seasonal anomalies in rainfall amount are found to be intrinsically noisy across Monsoonal India, while seasonal anomalies in daily rainfall frequency are more spatially coherent (Table 3, Fig. 14). The noisiness of local seasonal amounts suggests an intrinsic seasonal predictability limit, while rainfall frequency can be expected to be more seasonally predictable, consistent with previous findings for India and other tropical regions (Moron et al. 2006, 2007; Robertson et al. 2006, 2009). Despite this differing behavior between seasonal rainfall amounts and frequencies at local scale, the interannual variations of their spatial averages match almost perfectly. This implies that seasonal frequencies and amounts share the same common signal, which is rather homogeneous across Monsoonal India, except perhaps in the northeastern corner of the domain (Fig. 14). Thus, their (seasonal) predictability is comparable when pooling over the entire domain, while at any particular location the rainfall frequency is considerably more predictable than seasonal rainfall total.

Higher spatial coherence of decadal rainfall anomalies found during the onset and withdrawal phases of the 11 wettest and 11 driest years provides more evidence that these periods are inherently more predictable at seasonal lead times compared to the core of the monsoon (Fig. 15). Similar behavior was also found when looking at changes in HMM rainfall state frequency and MAC intensity

between these two subsets of years (Fig. 14). Thus, the monsoon predictive skill at monthly lead times and longer is likely to be limited from June to mid-July, and mid-August onward. Consistent with these findings, skillful dynamical extended-range hindcasts of June rainfall over India have recently reported by Vitart and Molteni (2009), while Vitart et al. (2008) found that a dynamical seasonal forecasting system only exhibited skill for the monsoon period from August onward.

The MAC and ISO components together capture just over half the raw daily OLR variance, with the remainder including the quasi-biweekly mode (QBM), as well as synoptic-and smaller-scale variance, all of which act to limit local-scale predictability on longer time scales. The contribution of the QBM may be important north of the Bay of Bengal, where its variance is strongest (Hoyos and Webster 2007; Krishnamurthy and Shukla 2008), while relationships between mesoscale to synoptic-scale phenomena and the MAC and ISO remain to be analyzed.

Finally, it seems worth mentioning that M-SSA, in combination with the maximum entropy method (recall Fig. 1 here) could lead to highly competitive prediction skill of those features of the phenomena analyzed here that do capture substantial variance of the rainfall amounts or frequencies. Indeed, this combination has been proven to be quite successful in predicting certain features of the El Niño–Southern Oscillation phenomenon in the Eastern Tropical Pacific (Keppenne and Ghil 1992; Ghil and Jiang 1998; Ghil et al. 2002). We expect that similar success could be encountered in this context, especially when combining this spectral approach for the large-scale features with the HMM one used in characterizing the rainfall states.

Acknowledgments. We are grateful to M. Rajeevan and the India Meteorological Department for supplying the Indian rainfall data set. Interpolated OLR data were provided by the Physical Sciences Division (PSD) of the Earth System Research Laboratory (ESRL) of the National Oceanic and Atmospheric Administration (NOAA), in Boulder, Colorado, USA, from their Web site at

http://www.esrl.noaa.gov/psd/data/gridded/data.interp_OLR.html. The NHMM software (MVNHMM) was developed by S. Kirshner and can be obtained free of charge from http://www.stat.purdue.edu/~skirshne/MVNHMM/. This research was supported by grant NA050AR4311004 from the National Oceanic and Atmospheric Administration (NOAA) to Columbia University (AWR) and by the Department of Energy's grant DE-FG02-07ER64439 from its Regional and Global Climate Modeling (RGCM) Program to UCLA (MG). Interaction between the authors was facilitated by a grant from the Institut Universitaire de France to VM. We thank the three reviewers for their suggestions that help us to improve the readability of the manuscript.

References

Ajaya Mohan RS, Goswami BN (2000) A common spatial mode for intra-seasonal and inter-annual variation and predictability of the Indian summer monsoon. Curr Sci 79:1106-1111.

Ajaya Mohan RS, Goswami BN (2007) Dependence of simulation of boreal summer tropical intraseasonal oscillations on the simulation of seasonal mean, J Atmos Sci 64:460-478.

Ajaya Mohan RS, Annamalai H, Luo JJ, Hafner J, Yamagata T (2010) Poleward propagation of boreal summer intraseasonal oscillations in a coupled model: role of internal processes. Clim Dyn. doi: 10.1007/s00382-010-0839-6./NCAR

Annamalai H, Slingo JM, Sperber KR, Hodges K (1999) The mean evolution and variability of the Asian summer monsoon: comparison of ECMWF and NCEP Reanalyses. Mon Wea Rev 127:1157-1186.

Annamalai H, Slingo JM (2001) Active/break cycles: diagnosis of the intraseasonal variability of the Asian summer monsoon. Clim Dyn 18:85-102.

Bhanu Kumar OSRU, Ramalingeswara Rao S, Ranganathan S, Raju SS (2010) Role of Intra-seasonal oscillations on Monsoon floods and droughts over India. Asia-Pacific J Atmos Sci 46:21-28.

Bhat GS (2006) The Indian drought of 2002 – a subseasonal phenomenon ? Quart J R Meteo Soc 132:2583-2602.

Brankovic C, Palmer TN (2000) Seasonal skill and predictability of ECWMF PROVOST ensembles. Quart J R Meteo Soc 126:2035-2067.

Chang CP, Wang Z, McBride J, Liu CH (2005) Annual cycle of Southeast Asia–Maritime Continent rainfall and the asymmetric monsoon transition. J Clim 18:287-301.

Chatterjee P, Goswami BN (2004) Structure, genesis and scale selection of the tropical qausi-biweekly mode. Quart J R Meteo Soc 130:1171-1194.

Chen TC, Chen JM (1993) The 10-20 day mode of the 1979 Indian monsoon; its relation with the time variation of monsoon rainfall. Mon Wea Rev 121:2465-2482.

Dempster AP, Laird NM, Rubin DR (1977) Maximum Likelihood from incomplete data via the EM algorithm. J R Stat Soc, B39:1-38.

Fennessy MJ, Kinter III JL, Kirtman B, Marx L, Nigma S, Schneider E, Shukla J, Straus D, Vernekar A, Xue Y, Zhou J (1994) The simulated Indian monsoon: a GCM sensivity study. J Clim 7: 33-43.

Ferranti L, Slingo JM, Palmer TN, Hoskins BJ (1997) Relations between interannual and intraseasonal monsoon variability as diagnosed from AMIP integrations. Quart J R Meteo Soc 123:1323-1357.

Forney Jr GD (1978) The Viterbi algorithm. Proc IEEE 61:268-278.

Fujinami H, Hatsuzuka D, Yasunari T, Hayashi T, Terao T, Murata F, Kiguchi M, Yamane Y. Matsumoto J, Nazrul Islam Md, Habib A (2011) Characteristic intraseasonal oscillation of rainfall and its effect on interannual variability over Bangladesh during boreal summer. Int J Climatol 31:1192-1204. doi:10.1002/joc.2146.

Gadgil S (2003) The Indian monsoon and its variability. Ann Rev Planet Sci 31:429-467.

Gadgil S, Sajani S (1998) Monsoon precipitation in the AMIP runs. Clim Dyn 14: 659-689.

Gadgil S, Joseph PV (2003) On breaks of the Indian monsoon. Proc Ind Acad Sci (Earth Planet Sci) 112:529-558.

Ghahramani Z (2001) An introduction to hidden Markov models and Bayesian networks. Int J Pattern Recogn Art Intell 15:9-42. doi:10.1142/S0218001401000836.

Ghil M, Allen MR, Dettinger MD, Ide K, Kondrashov D, Mann ME, Robertson AW, Saunders A, Tian Y, Varadi F, Yiou P (2002) Advanced spectral methods for climatic time series. Rev Geophys 40: 1003. doi:10.1029/2000RG000092.

Ghil, M, Jiang N (1998) Recent forecast skill for the El Niño/Southern Oscillation. Geophys Res Lett 25:171-174.

Ghil, M, Robertson AW (2002) "Waves" vs. "particles" in the atmosphere's phase space: A pathway to long-range forecasting? Proc Natl Acad Sci 99 (Suppl. 1):2493-2500.

Goddard L, Barnston AG, Mason SJ (2003) Evaluation of the IRI's “Net assessment” seasonal climate forecasts: 1997-2001. Bull Amer Meteo Soc 84:1761-1781.

Goswami BN (2005) South Asian monsoon. In Intraseasonal Variability in the Atmosphere-Ocean Climate System, Eds. W.K.M. Lau and D.E. Walliser, Springer, 21-61.

Goswami BN, Sengupta D, Suresh Kumar G (1998) Intraseasonal oscillations and interannual variability of surface winds over the Indian monsoon region. Proc Ind Acad Sci 107:45-64.

Goswami BN, Ajaya Mohan RS (2001) Intraseasonal oscillations and interannual variability of the Indian summer monsoon. J Clim 14:1180-1196.

Goswami BN, Xavier PK, Sengupta D (2003) Clustering of synoptic activity by Indian monsoon intraseasonal oscillations. Geophys Res Lett 30. doi:10.1029/2002GL016734.

Goswami BN, Wu G, Yasunari T (2006) The annual cycle, intraseasonal oscillations, and roadblock to seasonal predictability of the Asian summer monsoon. J Clim 19:5078-5099.

Greene AM, Robertson AW, Kirshner S (2008) Analysis of Indian monsoon daily rainfall on subseasonal to multidecadal time scales using a Hidden Markov Model. Quart J R Meteo Soc 134:875-887.

Greene AM, Robertson AW, Smyth P, and Triglia S (2011) Downscaling projections of Indian monsoon rainfall using a non-homogeneous hidden Markov model. Quart J R Meteo Soc 137:347-359.

Hartmann DL, Michelsen ML (1989) Intraseasonal periodicities in Indian rainfall. J Atmos Sci 46:2838-2862.

Hoyos CD, Webster PJ (2007) The role of intraseasonal variability in the nature of Asian monsoon precipitation. J Clim 20:4402-4424.

Hughes JP, Guttorp P (1994) A class of stochastic models for relating synoptic atmospheric patterns to regional hydrologic phenomena. Water Res Res 30:1535-1546.

Janicot S, Moron V, Fontaine B (1996) ENSO and Sahel droughts. Geophys Res Lett 23:515-518.

Jian X, Li T, Wang B (2003) Structures and mechanisms of the northward propagating boreal summer intraseasonal oscillations. J Clim 17:1022-1039.

Joseph PV, Simon A, Nair VG, Thomas A (2004) Intra-seasonal oscillation (ISO) of south Kerala rainfall during the summer monsoons of 1901–1995. Proc Indian Acad Sci 113:139-150.

Joseph S, Sahai AK, Goswami BN (2010) Boreal summer intraseasonal oscillations and seasonal Indian monsoon prediction in DEMETER coupled models. Clim Dyn. doi:10.1007/s00382-009-0635-3.

Kalnay E, Kanamitsu M, Kistler R, Collins W, Deaven D, Gandin L, Iredell M, Saha S, White G, Woollen J, Zhu Y, Leetmaa A, Reynolds R, Chelliah M, Ebisuzaki W, Higgins W, Janowiak J, Mo KC, Ropelewski C, Wang J, Jenne R, Joseph D (1996) The NCEP/NCAR 40-year reanalysis project. Bull Amer Meteo Soc 77:437-471.

Kang IS, Ho CH, Lim YK, Lau KM (1999) Principal modes of climatological seasonal and intraseasonal variations of the Asian summer monsoon. Mon Wea Rev 127:322-340.

Keppenne CL, Ghil M (1992) Adaptive filtering and prediction of the Southern Oscillation index. J Geophys Res 97:20449-20454.

Klingaman NP, Weller H, Slingo JM, Inness PM (2008) The intraseasonal variability of the Indian monsoon using TMI sea surface temperatures and ECMWF Reanalysis. J Clim 21:2519-2538.

Kripalani RH, Kulkarni A, Sabade SS, Revadekar JV, Patwardhan SK, Kulkarni JR (2004) Intrasea-

sonal oscillations during monsoon 2002 and 2003. Current Sci 87:325-331.

Krishna Kumar K, Soman MK, and K Rupa Kumar (1995) Seasonal forecasting of Indian summer rainfall. Weather 50:449-467.

Krishna Kumar K, Rupa Kumar K, Ashrit RG, Deshpande NR, Hansen JW (2004) Climate impacts on Indian agriculture. Int J Climatol 24:1375-1393.

Krishnamurthy V, Shukla J (2000) Intraseasonal and interannual variability of rainfall over India. J Clim 13:4366-4377.

Krishnamurthy V, Shukla J (2007) Intraseasonal and seasonally persisting patterns of Indian monsoon rainfall. J Clim 20:3-20.

Krishnamurthy V, Shukla J (2008) Seasonal persistence and propagation of intraseasonal patterns over the Indian monsoon region. Clim Dyn 30:353-369.

Krishnamurti TN, Balme HN (1976) Oscillations of a monsoon system. Part I. Observational aspects. J Atmos Sci 33: 1937-1954.

Krishnamurti TN, Bedi HS, Subramaniam M (1989) The summer monsoon of 1987. J Clim 2:321-340.

Krishnamurti TN, Ardanuy P, Ramanathan Y and Pasch R (1981) On the onset vortex of the summer monsoon. Mon Wea Rev 109:344-363.

Krishnan R, Venkatesan C (1996) Mechanisms of low frequency intraseasonal oscillations of the Indian summer monsoon, Meteo Atmos Phys 62:101-128.

Kulkarni A, Sabade SS, Kripilani RH (2009) Spatial variability of intra-seasonal oscillations during extreme Indian monsoons. Int J Climatol 29:1945-1955. doi:10.1002/joc.1844.

Lau KM, Chan PH (1986) Aspects of 30-50 day oscillation during summer as inferred from outgoing longwave radiation. Mon Wea Rev 114:1354-1369.

Lawrence DM, Webster PJ (2001) Interannual variations of the intraseasonal oscillation in the

South Asian summer monsoon region. J Clim 14:2910-2922.

Lawrence DM, Webster PJ (2002) The boreal summer intraseasonal oscillation; relationship between northward and eastward movement of convection. J Atmos Sci 59:1593-1606.

Liebmann B, Smith CA (1996) Description of a complete (interpolated) outgoing longwave radiation dataset. Bull Amer Meteo Soc 77:1275-1277.

Meehl G (1987) The annual cycle and interannual variability in the tropical Pacific and Indian ocean regions. Mon Wea Rev 115:27-50.

Mitra AK, Stefanova L, Vijaya Kumar TSV, Krishnamurti TN (2005) Seasonal prediction for the Indian monsoon region with FSU ocean-atmosphere coupled model: model mean and 2002 anomalous drought, Pure and Applied Geophys 162:1431-1454.

Mohapatra M, Mohanty UC (2008) Peridiodicity in intraseasonal variation of summer monsoon rainfall over Orissa, India in relation with synoptic disturbances. Meteorol Atmos Phys 99:25-42.

Mooley DA, Parthasarathy B (1984) Fluctuations in All-India summer monsoon rainfall during 1871-1978. Climate Change 6:287-301.

Moron V, Vautard R, Ghil M (1998) Trends, decadal and inter-annual variability in global sea surface temperature fields. Clim Dyn 14:545-569.

Moron V, Robertson AW, Ward MN (2006) Seasonal predictability and spatial coherence of rainfall characteristics in the tropical setting of Senegal. Mon Wea Rev 134:3248-3262.

Moron V, Robertson AW, Ward MN, Camberlin P (2007) Spatial coherence of tropical rainfall at the regional scale. J Clim 20:5244-5263.

Moron V, Robertson AW, Boer R (2009) Spatial coherence and seasonal predictability of monsoon onset over Indonesia. J Clim 22:840-850.

Munot AA, Kothawale DR (2000) Intra-seasonal inter-annual and decadal scale variability in sum-

mer monsoon rainfall over India. Int J Climatol 20:1387-1400.

Murakami T (1976) Analysis of summer monsoon fluctuations over India. J Meteor Soc Japan 54:15-31

Murakami T, (1980) Empirical orthogonal function analysis of Satellite-Observed outgoing long-wave radiation during summer. Mon Wea Rev 108:205-222.

Murakami T, Nakazawa T (1985) Tropical 45 day oscillations during the 1979 Northern Hemisphere summer. J Atmos Sci 42:1107-1122.

Pai DS, Bhate J, Sreejith OP, Hatwar HR (2011) Impact of MJO on the intraseasonal variation of summer monsoon rainfall over India. Clim Dyn 36:41-55. doi:10.1007/s00382-009-0634-4.

Parthasarathy B, Rupa Kumar K, Munot AA (1993) Homogenous Indian monsoon rainfall: variability and prediction. Proc Ind Acad Sci (Earth Plan Sci) 102:121-155.

Parthasarathy B, Munot AA, Kothawale DK (1995) All-India monthly and seasonal rainfall series: 1871-1993. Theor App Climatol 49:217-224.

Pattanaik DR, Kumar A (2010) Prediction of summer monsoon rainfall over India using the NCEP climate forecast system. Clim Dyn 4:557-572. doi: 10.1007/s00382-009-0648-y.

Plaut G, Vautard R (1994) Spells of low-frequency oscillations and weather regimes in the Northern Hemisphere. J Atmos Sci 51:210-236.

Prasad KD, Singh SV (1996) Forecasting the spatial variability of the Indian monsoon rainfall using canonical correlation. Int J Climatol 16:1379-1390.

Preethi B, Kripalani RH, Krishna Kumar K (2010) Indian summer monsoon rainfall variability in global ocean-atmospheric models. Clim Dyn 35:1521-1533. doi 10.1007/s00382-009-0657-x

Qi YJ, Zhang RH, Li T, and M Wen (2009) Impacts of intraseasonal oscillation in the onset and interannual variation of the Indian summer monsoon. Chinese Sci Bull 54:880-884.

Rajeevan M, Bhate J, Kale J, Lal B (2005) Development of a High resolution daily gridded rainfall data for the Indian region. Met. Monograph Climatology n° 22/2005. India Meteorological Department.

Rajeevan M, Bhate J, Kale JD, Lal B (2006) A high resolution daily gridded rainfall for the Indian region: analysis of break and active monsoon spells. Curr Sci 91:296-306.

Rajeevan M, Gadgil S, Bhate J (2008) Active and break spells of the Indian summer monsoon, NCC research report n°7, India Meteorological Department, 46 p.

Robertson AW, Kirshner S, Smyth P (2004) Downscaling of daily rainfall occurrence over North-East Brazil using a Hidden Markov Model. J Clim 17:4407-4424.

Robertson AW, Kirshner S, Smyth P, Charles SP, Bates BC (2006) Subseasonal-to-interdecadal variability of the Australian monsoon over North Queensland. Quart J R Meteo Soc 132:519-542.

Robertson AW, Moron V, Swarinoto Y (2009) Seasonal predictability of daily rainfall statistics over Indramayu district, Indonesia. Int J Climatol 29: 1449-1462.

Saith N, Slingo J (2006) The role of the Madden-Julian oscillation in the El Nino and Indian drought of 2002. Int J Climatol 26:1361-1378.

Sajani S, Naseema Beegum S, Krishna Moorthy K (2007) The role of low-frequency intraseasonal oscillations in the anomalous Indian summer monsoon rainfall of 2002. J Earth Syst Sci 116:149-157.

Sanjeeva Rao P, Sikka DR (2005) Intraseasonal variability of the summer monsoon over the North Indian ocean as revealed by the BOBMEX and ARMEX field programs. Pure Applied Geophys 162:1481-1510.

Sengupta DB, Goswami BN, Senan R (2001) Coherent intraseasonal oscillations of ocean and atmosphere during the Asian summer monsoon. Geophys Res Lett 28:4127-4130.

Sikka DR, Gadgil S (1980) On the maximum cloud zone and the ITCZ over India longitude during the Southwest monsoon. Mon Wea Rev 108:1840-1853.

Singh SV, Kripilani RH (1985) The South to North progression of rainfall anomalies across India during the summer monsoon season, Pure Applied Geophys 123:624-637.

Singh SV, Kripalani RH (1986) Application of extended empirical orthogonal function analysis to interrelationships and sequential evolution of monsoon fields. Mon Wea Rev 114:1603-1610.

Singh SV, Kripilani RH, Sikka DR (1992) Inter-annual variability of the Madden-Julian oscillations in Indian summer monsoon rainfall. J Clim 5:973-978.

Sivakumar MVK (1988) Predicting rainy season potential from the onset of rains in southern Sahelian and Sudanian climatic zones of West Africa. Agric For Meteo 42:295-305.

Slingo J, Annamalai H (2000) The El Nino of the century and the response of the Indian Summer Monsoon. Mon Wea Rev 128: 1778-1787.

Sperber K.R, Slingo J, and H. Annamalai (2000) Predictability and the relationship between subseasonal and interannual variability during the Asian summer monsoon. Quart J R Meteo Soc 126:2545-2574.

Sperber KR, Annamalai H (2008) Coupled model simulations of boreal summer intraseasonal (30-50 day) variability, Part 1: systematic errors and caution on use of metrics. Clim Dyn 31:345-372.

Vecchi GA, Harrison DE (2002) Monsoon breaks and subseasonal sea surface temperature variability in the Bay of Bengal. J Clim 15:1485-1493.

Vernekar AD, Thapliyal V, Kripalani RH, Singh SV, Kirtman B (1993) Global structure of the Madden-Julian oscillations during two recent contrasting summer monsoon seasons over India. Meteo Atm Phys 52:37-47.

Vitart F, Molteni F (2009) Dynamical extended-range prediction of early monsoon rainfall over India. Mon Wea Rev 137:1480-1492.

Vitart F, Molteni F, Stockdale T, Ferranti L, Balmaseda M (2008) Predictions of tropical rainfall with the ECMWF seasonal and monthly forecast systems. Proc. Workshop on Ensemble Prediction, Reading, United Kingdom, ECMWF. [available online at http://www.ecmwf.int/publications/library/ecpublications/_pdf/workshop/2007/Ensemble_prediction/Molteni.pdf]

Walliser DE, Stern W, Schubert S, Lau KM (2003) Dynamic predictability of intraseasonal variability associated with the Asian summer monsoon. Quart J R Meteo Soc 129:2897-2925.

Wang B, Xie X (1997) A model for the boreal summer intraseasonal oscillation. J Atmos Sci 54:71-86.

Wang B, Xu XH (1997) Northern Hemisphere summer monsoon singularities and climatological intraseasonal oscillation. J Clim 10:1071-1085.

Wang B, LinHo (2002) Rainy season of the Asian-Pacific summer monsoon. J Clim 15: 386-398.

Webster PJ, Yang S (1992) Monsoon and ENSO: selectively interactive systems. Quart J R Meteo Soc 118:877-920.

Webster PJ, Magana VO, Palmer TN, Shukla J, Tomas RA, Yanai M, Yasunari T (1998) Monsoons: processes, predictability and the prospects for prediction. J Geophys Res 103:14451-14510.

Wheeler MC, Hendon HH (2004) An all-season real-time multivariate MJO index: development of an index for monitoring and prediction. Mon Wea Rev 132:1917-1932.

Wu Z, Schneider EK, Kirtman B, Sarachik ES, Huang NE, Tucker CJ (2008) The modulated annual cycle: an alternative reference frame for climate anomalies. Clim Dyn 31:823-841.

Xavier PK, Marzin C, Goswami BN (2007) An objective definition of the Indian summer monsoon season and a new perspective of the ENSO-monsoon relationship. Quart J R Meteo Soc 133:

749-764. doi:10.1002/qj.45.

Yasunari T (1979) Cloudiness fluctuations associated with the northern hemisphere summer season. J Meteo Soc Japan 57:227-242.

Yasunari T (1980) A quasi-stationary appearance of 30 to 40 day period in the cloudiness fluctuations during the summer monsoon over India. J Meteo Soc Japan 58:225-229.

Yasunari T (1981) Structure of an Indian summer monsoon system with around 40-day period. J Meteo Soc Japan 59:336-354.

Yoo JH, Robertson AW, Kang IS (2010) Analysis of intraseasonal and interannual variability of the Asian monsoon using a hidden Markov model. J Clim 23: 5498-5516.

Figure legends

Figure 1: Power spectra of the ten leading space-time principal components (ST-PCs) from multichannel singular spectrum analysis (M-SSA) of daily outgoing long-wave radiation (OLR) and zonal and meridional components of the 925-hPa winds. The spectra were computed separately for each ST-PC by using the maximum entropy method with a 60-day window over Monsoonal India (60°–100°E, 0–35°N); the legend in the figure gives the key to individual-PC results. The missing period from March 17 to December 31, 1978, in the OLR data set is replaced with the OLR mean seasonal cycle computed on the available data. Mean and standard deviations are computed for the whole available period and used to normalize the anomalies. An empirical orthogonal function (EOF) analysis is then applied to the standardized anomalies of OLR and wind to retain 75% of the entire variance, which yields the 22 leading principal components (ordinary, spatial-only PCs). Solely spectral peaks that are significant according to a Monte Carlo test with 1000 realizations of an auto-regressive process of order one (AR1 or "red noise") are displayed.

Figure 2: (a) Ratio of variance in daily OLR data, during the June-to-September (JJAS) season, captured by the intraseasonal oscillation (ISO) — defined as the sum of the space-time reconstructed components (ST-RCs) 5-6 of the M-SSA in Fig. 1 — and the variance captured by the modulated annual cycle (MAC) — given by the sum of ST-RCs 1–4 of the same analysis. (b) Time-latitude diagram of the daily mean of ISO amplitude, defined as the daily standard deviation of the ST-RCs 5–6 averaged between 60° and 100°E; units are the standard deviations.

Figure 3: Time-latitude diagram of the longitudinal mean (60°–100°E) for the dry year 1987 of (a) daily OLR (in Wm^{-2}); (b) MAC (RCs 1–4); and (c) ISO (RCs 5–6) from the M-SSA reported in Fig. 1. Units in panels (b) and (c) are anomaly (in Wm^{-2}) relative to the long-term mean.

Figure 4: Phase composites of the MAC defined as the sum of the space-time reconstructed components 1-4 of the M-SSA in Fig. 1; OLR standardized anomalies shown as shadings and standardized anomalies of the zonal and meridional components of the 925-hPa winds shown as vectors. The eight phases are computed relative to the spatial average of MAC OLR over Monsoonal India (see

text). The phases occur at least 50% of years during the time window noted in the title of each panel.

Figure 5: Same as Fig. 4, but for the ISO, defined as the sum of the space-time reconstructed components 5-6 of the M-SSA in Fig. 1. The eight phases are still computed from the ISO average of OLR over Monsoonal India; same plotting conventions as in Fig. 4.

Figure 6: MAC (black full line) and its climatological long-term mean (black dashed line) and the ISO (red full line) of daily OLR and daily rainfall (grey bars) in the dry years (a) 1987 and (c) 2002, and the two wet years (b) 1988 and (d) 2003. The scalar indices of MAC and ISO here are estimated as spatial averages of the ST-RCs 1–4 and 5-6, respectively, across Monsoonal India from M-SSA of Fig. 1. The spatial averages are multiplied by -1 so that positive MAC and ISO anomalies should correspond to positive rainfall anomalies. Daily rainfall values (in mm/day) are averaged over the same area as for the OLR and ISO data; for ease of comparison with the M-SSA results, we multiplied the time series by 3.

Figure 7: Characteristics of the three Hidden Markov Model (HMM) states obtained, during wet days: (a–c; left column) probability (shadings) and probability anomaly in % (contours); and (d–f, right column) mean rainfall (shadings) and mean rainfall anomaly in % (contours); computed from daily rainfall during JJAS for the full data set (1975–2008) across Monsoonal India.

Figure 8: Standardized anomalies of OLR (shadings) and 925-hPa winds (vectors) for (a) State 1, (b) State 2, and (c) State 3. The daily values of OLR and 925 hPa are standardized to zero mean and unit variance over all 34 July–September seasons, 1975–2008.

Figure 9: Viterbi sequence of the three hidden Markov model (HMM) states with “active” and “break” days superimposed as black and red squares respectively from Rajeevan et al. (2008) for 1975-2007 (July-August). State 1 is shown as green squares, State 2 as blue squares, and State 3 as yellow squares.

Figure 10: Significant frequency of the HMM model, according to the standardized value of the spatial average of ISO across Monsoonal India (on the abscissa) and that of MAC (on the ordinate),

during the JJAS monsoon season. The spatial averages of MAC/ISO are multiplied by -1, so that positive values should correspond to positive rainfall anomalies: (a) State 1, (b) State 2, and (c) State 3. The top row in the display shows the frequency of each HMM state according to the standardized value of the spatial average of ISO across Monsoonal India, while the rightmost column corresponds to that given by the marginal MAC distribution. The black plus sign indicates significant positive anomalies at the two-sided 90% level, according to a Monte Carlo test based on reshuffling the Viterbi sequence 1000 times (see text for details), while the white asterisks are for significant negative anomalies; the larger symbols indicate an absolute number of occurrences of at least 30 days.

Figure 11: Deviations between observed and expected frequency of HMM state for the eight ISO phases plotted in Fig. 5. The values are expressed as relative deviations from the expected frequency and the asterisks indicate significant values at the two-sided 90% level according to the same Monte Carlo test as in Fig. 10; color convention for the three states is the same as in Fig. 9.

Figure 12: Spatial average (across Monsoonal India) of the dates for (a) onset (light solid with open circles) and withdrawal (light solid with open squares), based on the mean deviation of the local-scale MAC with respect to its climatological long-term. (b) MAC intensity in June–September (JJAS; light solid with open squares), and its residuals from onset and withdrawal dates of the MAC (light solid with open circles). (c) JJAS standard deviations of ISO. (d) Standardized anomaly index (SAI) — i.e, the spatial average of the standardized anomalies across Monsoonal India — of the JJAS rainfall amounts across Monsoonal India. Horizontal dashed lines are the upper and lower terciles. In panels (a–c), the red and blue markers indicate the 11 driest and wettest years, respectively.

Figure 13: (a) Standardized anomalies of local-scale onset dates across Monsoonal India (black dotted lines) with its spatial average (bold solid black line with open circles) and the standardized MAC anomalies of onset dates (bold solid red line with open circles). (b) Frequency of local-scale onset date according to the 8 phases of MAC and ISO, spatially averaged across Monsoonal India, after MAC OLR has been interpolated from the 2.5° grid to a 1° grid; size of open circles is propor-

tional to absolute frequency of local-scale onset across Monsoonal India.

Figure 14: Standardized anomalies of (a,b) seasonal JJAS rainfall; and (c,d) seasonal frequency of wet days with over 1 mm of precipitation for the 11 driest years (lower tercile) and the 11 wettest years (upper tercile), estimated through the standardized anomaly index (SAI: spatial average of standardized anomalies) of JJAS seasonal amounts across Monsoonal India — the black dots indicate significant anomalies at the two-sided 90% level according to 1000 random samplings of the 11 years chosen in the set of 34 years. (e,f) Probability of HMM states over 11-day sliding windows for lower- and upper-tercile years, expressed as deviation in days with respect to the long-term mean; the plus signs and dots indicate positive and negative anomalies, respectively, which are significant at the two-sided 90% level, according to 1000 random permutations of the Viterbi sequence, while the color convention for the three states is the same as in Figs. 9 and 11. (g,h) Mean daily value of MAC OLR spatially-averaged across Monsoonal India (multiplied by -1) for lower and upper terciles (black line) with the 90% confidence interval from 1000 samples of 11 years randomly chosen in the set of 34 years; plus signs and dots as in panels (e,f).

Figure 15: Standardized Anomaly Index (SAI) of (a) rainfall amounts, and (b) rainfall frequency of wet days with more than 1 mm of precipitation, by decades (Jun 1 refers to June 1–10, Jun 2 refers to June 11–20, etc.) in JJAS for the 11 driest (DRY in blue) and wettest (WET in red) years defined from the SAI of JJAS amounts across Monsoonal India. The dashed lines indicate the 90% confidence interval according to a random sampling of 11 years chosen in the set of 34 years, 1000 times for each decade.

Tables

Acronym	Nature	Definition
AIRI	Climate	All India Rainfall Index
AVHRR	Data	Advanced Very High Resolution Radiometer
CMAP	Data	Climate Prediction Center Merged Analysis of Precipitation
EOF	Method	Empirical Orthogonal Function
ERA	Center/Organization	European Center for Medium Weather Forecast Reanalyses
FFT	Method	Fast Fourier Transform
HMM	Method	Hidden Markov Model
GPCP	Data	Global Precipitation Climatology Project
ISO	Climate	Intra-seasonal oscillation
ISV	Climate	Intra-seasonal variability
ITCZ	Climate	Inter Tropical Convergence Zone
JJA	Climate	June–August
JJAS	Climate	June–September
MAC	Climate	Modulated Annual Cycle
MJO	Climate	Madden-Julian Oscillation
M-SSA	Method	Multi-channel Singular Spectrum Analysis
NCEP	Center/Organization	National Center for Environmental Prediction
NOAA	Center/Organization	National Oceanic and Atmospheric Administration
OLR	Data/Climate	Outgoing Longwave Radiation
PC	Method	Principal Component
PDO	Climate	Pacific Decadal Oscillation
POP	Method	Principal Oscillation Pattern
QBM	Climate	Quasi-Biweekly Mode
RC	Method	Reconstructed Component
SAI	Method	Standardized Anomaly Index
SST	Climate	Sea Surface Temperature
ST-EOF	Method	Space-Time Empirical Orthogonal Function
ST-PC	Method	Space-Time Principal Component
TMI	Data	TRMM Microwave Imager
TRMM	Data	Tropical Rainfall Measuring Mission

Table 1: Definition and nature of the acronyms used throughout the paper.

References	Main statistical method	Data set used (the Monsoon season is always June-September if not indicated)	Computation of anomalies and/or extraction of oscillation/annual cycle
Singh and Kripalani (1985)	Hovmoller diagram, correlation, Extended EOF	Daily rainfall data for 123 Indian stations (1955–1973) transformed into 2.5° (latitude) x 5° (longitude) blocks	Computation of pentad rainfall and subtraction of the long-term mean annual cycle and division by the long-term standard deviation
Singh and Kripalani (1986)	Extended EOF	Daily 700 hPa height (1958–1978), daily mean sea level pressure anomaly (1946–1975) and daily rainfall across India for 32 meteorological subdivisions (from 220 stations, 1966–1973) and weekly rainfall for these met. Subdivisions (1963–1982) for July-August	Computation of pentad rainfall and subtraction of long-term mean annual cycle
Singh et al. (1992)	Bandpass filtering (30–60 days)	Daily rainfall from 365 Indian stations (1901-1980) spatially averaged on 52 2.5° blocks (except along the Western Ghats)	NA
Hartmann and Michelsen (1989)	FFT spectrum	Daily rainfall over 1° grid-point (from 3700 rain gauges) from April 1st (1901–1970)	Subtraction of the long-term mean annual cycles smoothed with a 1-2-1 filter
Ajaya Mohan and Goswami (2000)	Power spectral estimates, bandpass filtering (30–60 days)	Daily winds from NCEP Reanalyses (1956-1997) and daily OLR (1974-1997) and daily value of AIRI	Subtraction of the annual cycle of each year (= sum of annual and semiannual harmonics)
Krishnamurty and Shukla (2000)	Analysis of variance, EOF	Daily rainfall over 1° grid-point (Hartmann and Michelsen 1989) (1901-1970)	Computation of pentad running mean and subtraction of the long-term mean annual cycle including and excluding seasonal anomaly
Munot and Kothawale (2000)	Blackman-Tukey spectrum	Daily rainfall over 52 2.5° blocks (Singh et al. 1992) spatially averaged into 5 homogeneous regions and all India in 1960–1989	Smoothing with a 3-day moving average
Sperber et al, (2000)	EOF	Daily NCEP reanalyses (1958-1997) and pentad CMAP rainfall (1979-1997)	Subtraction of the long-term mean annual cycle
Annamalai and Slingo (2001)	Bandpass filtering (10-20 and 20-60 days), POP	Daily OLR, daily ERA reanalyses anddaily AIRI (1979–1995)	Smoothing of Daily AIRI with a five-day running mean used as an index to define break/active periods.

Goswami and Ajaya Mohan (2001)	Power spectra, bandpass filtering (15-80 days), EOF and composite	Daily winds at 850, 500 and 200 hPa from NCEP reanalyses (1956-1997),daily OLR (1974-1997) anddaily gridded rainfall at 1.25° (1978–1989) in May-October	Extraction of annual cycle (= sum of the annual and semiannual harmonic) of each year
Lawrence and Webster (2001)	Bandpass filtering (25-80 days), EOF, wavenumber-frequency analysis	May-October daily gridded OLR (1979–1997)	NA
Joseph et al. (2004)	Wavelet	Daily rainfall (29th May to 3rd October) from 39–44 stations in South Kerala spatially averaged (1901–1995)	NA
Hoyos and Webster (2007)	Bandpass filtering (25-80 days), wavelet	6 regions (4 in India) Daily 1° rainfall from GPCP (1997-2004), 0.25° TRMM (1998-2005), daily OLR (1980-2005), TMI SST and Quikscat wind	NA
Krishnamurthy and Shukla (2007)	M-SSA and wavenumber – frequency spectral analysis	Gridded 1° daily rainfall (1901-1970)	Subtraction of the long-term mean annual cycle and then smoothing with a 5-day running mean
Klingaman et al. (2008)	Correlation and composites	Daily OLR, pentad CMAP rainfall , winds from ERA and ECMWF, TMI SST (1998-2005)	NA
Krishnamurthy and Shukla, (2008)	M-SSA and wavenumber-frequency spectral analysis	Daily OLR (1975-2002) + 1° grid-point daily rainfall (1951–2004) (Rajeevan et al. 2005)	Subtraction of the long-term mean annual cycle and then smoothing with 5-day running mean
Mohapatra and Mohanty (2008)	Auto-correlation and Blackman-Tukey spectra	Daily rainfall (1980–1999) for 31 stations in Orissa summarized by 6 homogeneous regions (defined using EOF)	NA
Kulkarni et al. (2009)	Multi Taper Method and wavelet, EOF analysis, composites	Daily rainfall spatially averaged over 4 representative regions in India (Krishnamurthy and Shukla 2000) (1951–2003), monthly PDO and Nino3 SST indices, AIRI (1871–2005)	NA
Qi et al. (2009)	Bandpass filtering (30-60 days) Composite and correlation	Daily OLR, NCEP Reanalysis and All India Rainfall index for (1975-2003)	NA
Bhanu Kumar et al. (2010)	Wavelet and Extended EOF	Daily winds at 850 and 200 hPa and daily OLR (1979–2006)	NA
Fujinami et al. (2011)	FFT, composite and regression	Daily rainfall in 25 stations in Bangladesh (JJA 1981-2000) spatially averaged, daily OLR and Japanese Reanalyses	Removing of the 3 first harmonics and 3-point running mean in the frequency domain

Pai et al. (2011)	Composite and phase-space diagram	1° grid-point daily rainfall (1951-2003) (Rajeevan et al. 2006), daily OLR and NCEP 850 hPa winds and MJO index of Wheeler and Hendon (2004)	Subtraction of the long-term mean annual cycle

Table 2: Summary of intraseasonal oscillation (ISO) studies. Acronyms for methods, data sources and phenomena are defined in table 1.

JJAS Monsoonal India	Mean	Variance [SAI]	% of seasonal rainfall
Seasonal amount	878 mm	0.16	NA
Mean intensity	15 mm/day	0.03	NA
Seas. Freq. ≥ 1 mm	56 days	0.31	99%
Seas. Freq. ≥ 10 mm	24 days	0.20	80%
Seas. Freq. ≥ 30 mm	8 days	0.09	44%
MAC intensity	NA	0.95	NA
MAC onset	NA	0.94	NA
MAC withdrawal	NA	0.91	NA
MAC length	NA	0.92	NA
ISO intensity	NA	0.93	NA

Table 3: Second column: spatial average of mean JJAS rainfall, daily mean intensity (= seasonal amount / seasonal frequency of wet days ≥ 1 mm), and frequency of wet days with precipitation ≥ 1 mm, ≥ 10 mm, and ≥ 30 mm. Third column: interannual variance of the spatial average of the standardized anomalies across Monsoonal India; this variance equals 1 for perfect in-phase variations and tends to zero for independent variations or out-of-phase variations between two equal samples (Moron et al. 2007). Fourth column: spatial average of the fraction of seasonal rainfall related to wet days with precipitation ≥ 1 mm, ≥ 10 mm, and ≥ 30 mm.

	JJAS rainfall	INT-MAC	ONSET	WITHDRAW	DURATION	INT-ISO
JJAS rainfall	100					
INT-MAC	65***	100				
ONSET	–24	–62***	100			
WITH	50***	62***	–14	100		
DURATION	47***	82***	–82***	68***	100	
INT-ISO	–24	–33*	1	–45***	–27	100

Table 4: Correlation (x 100) between the standardized anomaly index (= spatial average of standardized anomalies) of JJAS rainfall across Monsoonal India, the mean JJAS intensity of MAC (INT-MAC), the onset anomaly of MAC (ONSET), the withdrawal anomaly of MAC (WITHDRAW), the duration anomaly of MAC (DURATION) and the mean JJAS amplitude of ISO

(INT-ISO). One and three stars indicate significant correlation at the 90% and 99% two-sided level, respectively, according to a random-phase test (Janicot et al. 1996).

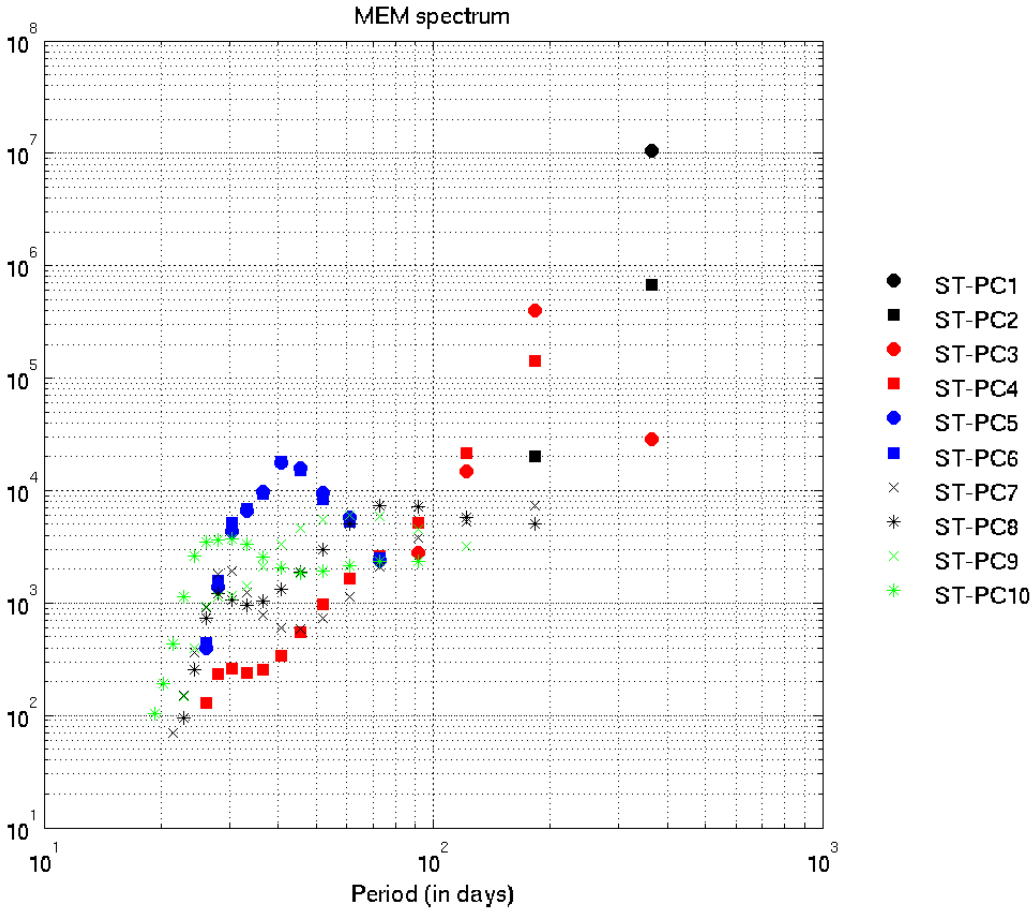
MEM spectrum
Period (in days)
ST-PC1
ST-PC2
ST-PC3
ST-PC4
ST-PC5
ST-PC6
ST-PC7
ST-PC8
ST-PC9
ST-PC10

FIGURE 1

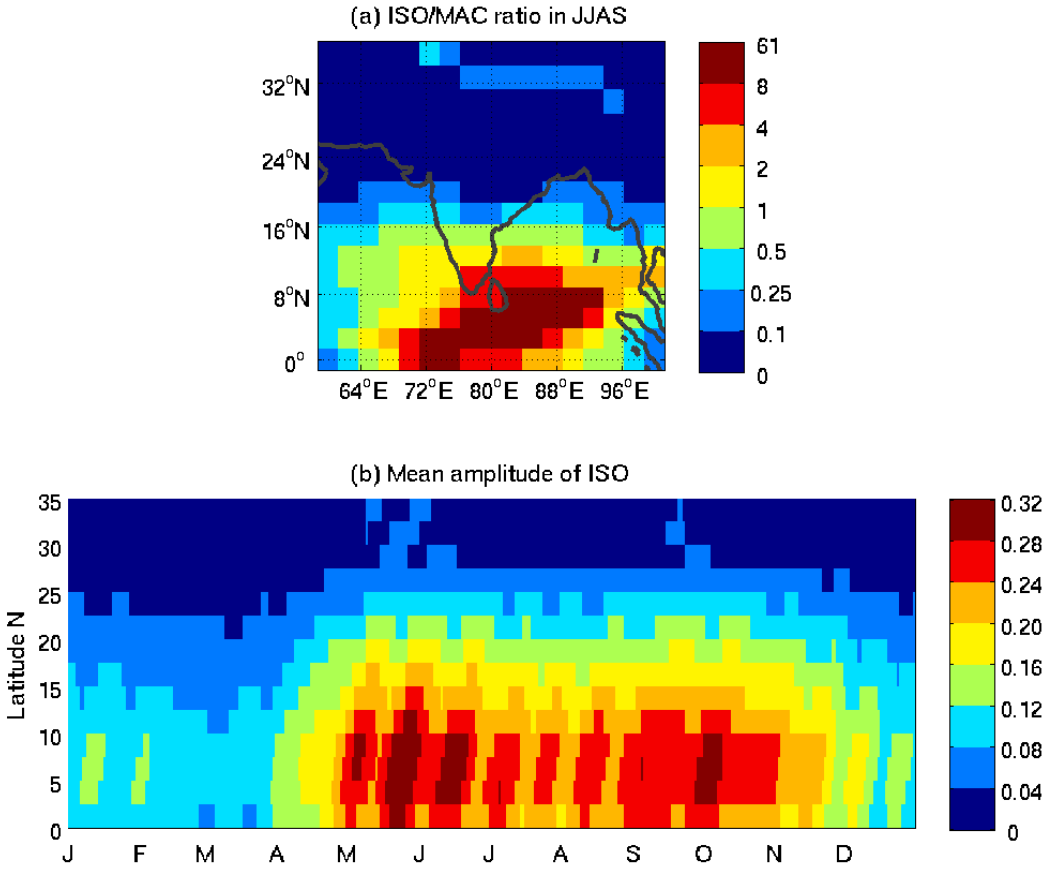
(a) ISO/MAC ratio in JJAS
32°N
24°N
16°N
8°N
0°
64°E 72°E 80°E 88°E 96°E
61
8
4
2
1
0.5
0.25
0.1
0
(b) Mean amplitude of ISO
Latitude N
35
30
25
20
15
10
5
0
J F M A M J J A S O N D
0.32
0.28
0.24
0.20
0.16
0.12
0.08
0.04
0

FIGURE 2

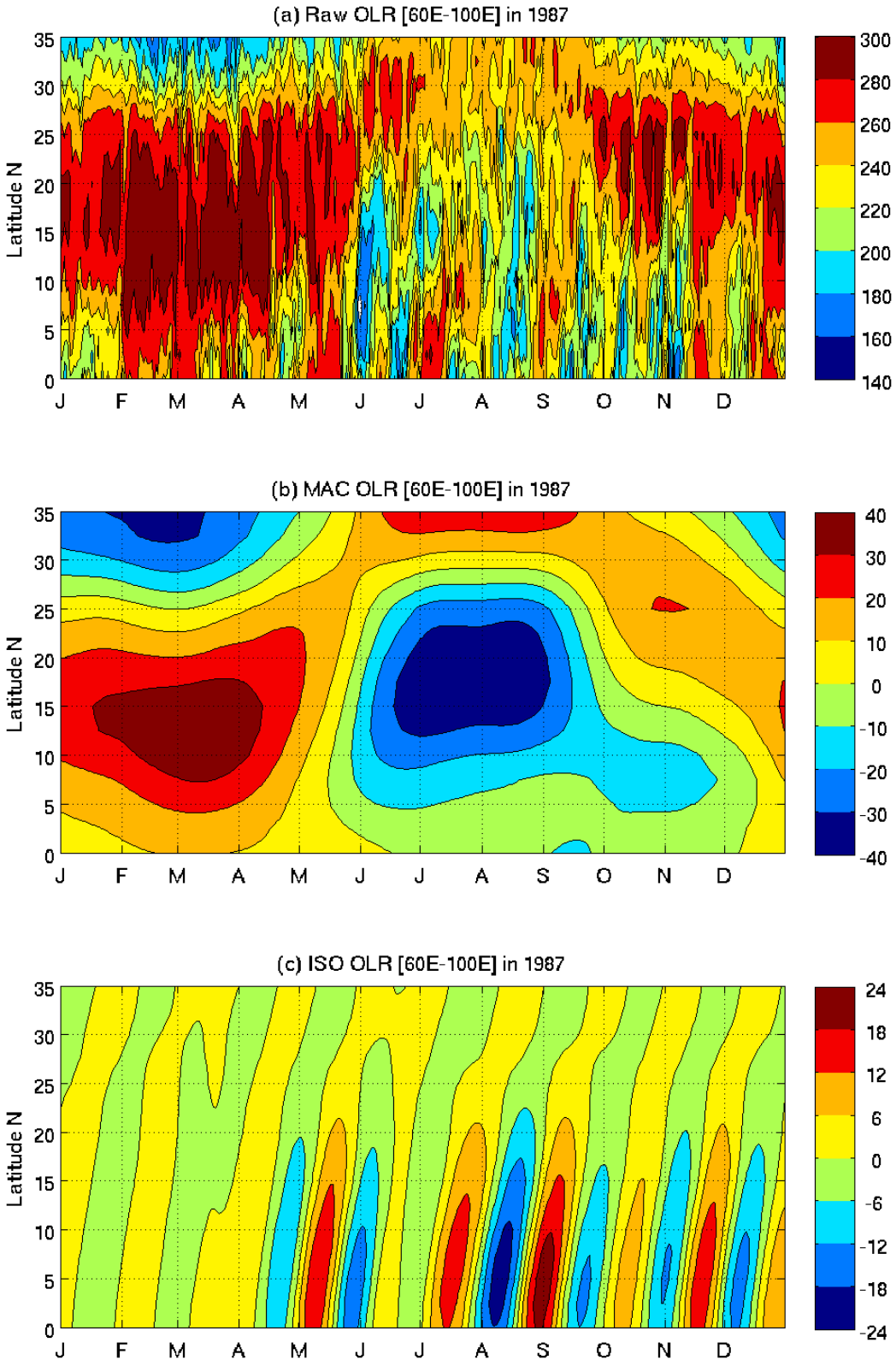
(a) Raw OLR [60E-100E] in 1987
Latitude N
0
5
10
15
20
25
30
35
J F M A M J J A S O N D
300
280
260
240
220
200
180
160
140
(b) MAC OLR [60E-100E] in 1987
Latitude N
0
5
10
15
20
25
30
35
J F M A M J J A S O N D
40
30
20
10
0
-10
-20
-30
-40
(c) ISO OLR [60E-100E] in 1987
Latitude N
0
5
10
15
20
25
30
35
J F M A M J J A S O N D
24
18
12
6
0
-6
-12
-18
-24

FIGURE 3

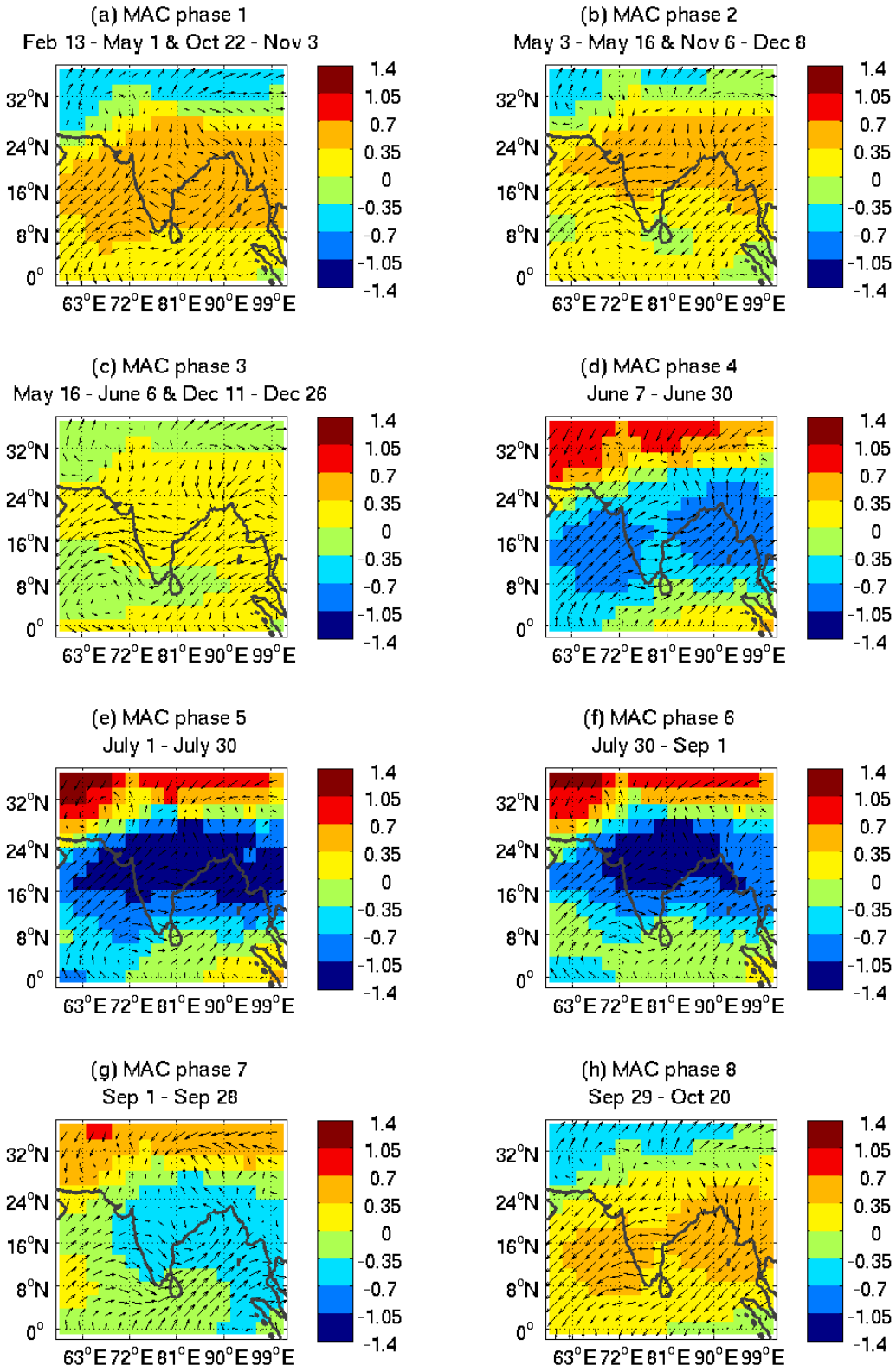
(a) MAC phase 1
Feb 13 - May 1 & Oct 22 - Nov 3
(b) MAC phase 2
May 3 - May 16 & Nov 6 - Dec 8
(c) MAC phase 3
May 16 - June 6 & Dec 11 - Dec 26
(d) MAC phase 4
June 7 - June 30
(e) MAC phase 5
July 1 - July 30
(f) MAC phase 6
July 30 - Sep 1
(g) MAC phase 7
Sep 1 - Sep 28
(h) MAC phase 8
Sep 29 - Oct 20
32°N
24°N
16°N
8°N
0°
63°E 72°E 81°E 90°E 99°E
1.4
1.05
0.7
0.35
0
-0.35
-0.7
-1.05
-1.4

FIGURE 4

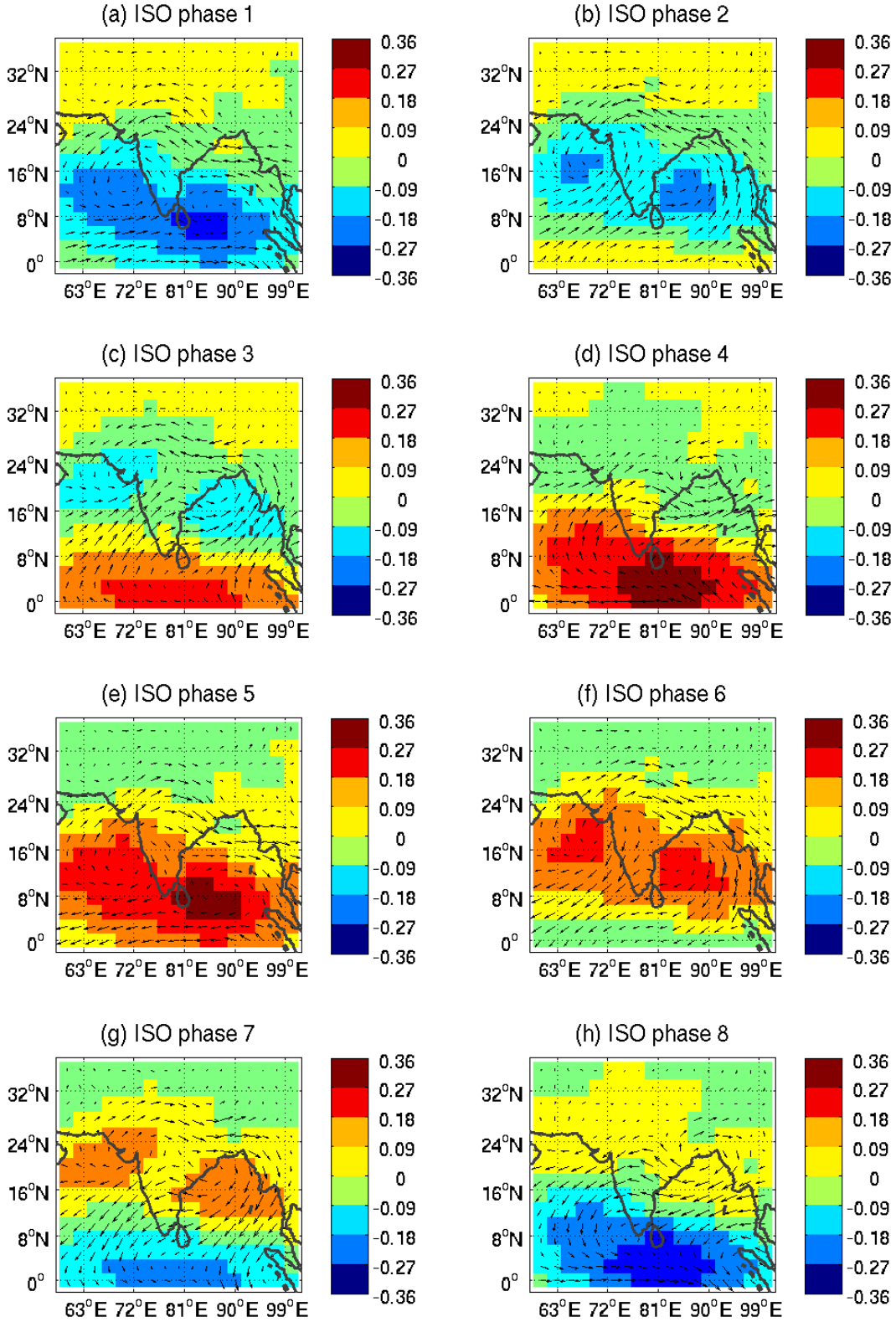
(a) ISO phase 1
(b) ISO phase 2
(c) ISO phase 3
(d) ISO phase 4
(e) ISO phase 5
(f) ISO phase 6
(g) ISO phase 7
(h) ISO phase 8
32°N
24°N
16°N
8°N
0°
63°E 72°E 81°E 90°E 99°E
0.36
0.27
0.18
0.09
0
-0.09
-0.18
-0.27
-0.36

FIGURE 5

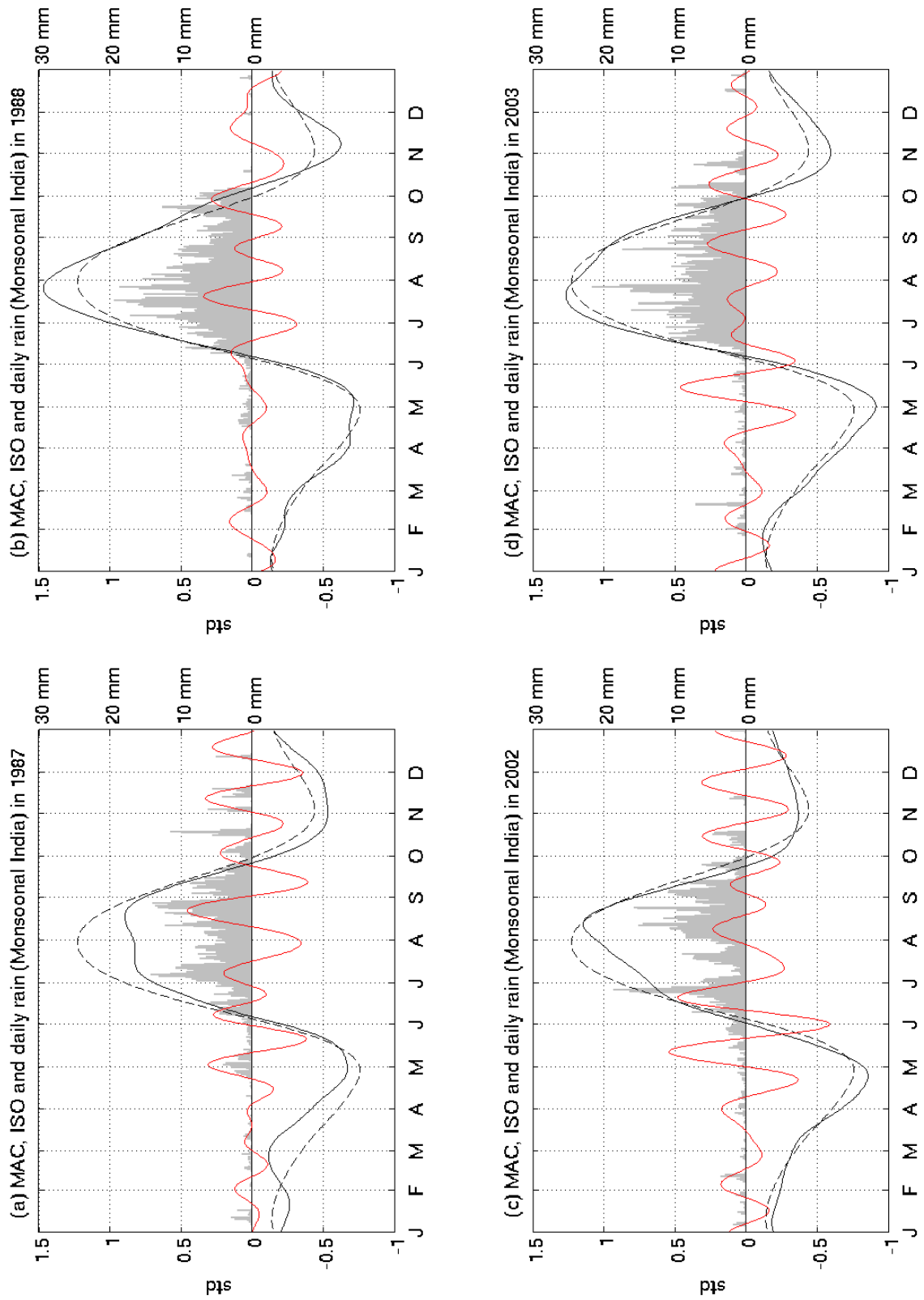
(a) MAC, ISO and daily rain (Monsoonal India) in 1987
(b) MAC, ISO and daily rain (Monsoonal India) in 1988
(c) MAC, ISO and daily rain (Monsoonal India) in 2002
(d) MAC, ISO and daily rain (Monsoonal India) in 2003
30 mm
20 mm
10 mm
0 mm
std
1.5
1
0.5
0
-0.5
-1
J F M A M J J A S O N D

FIGURE 6

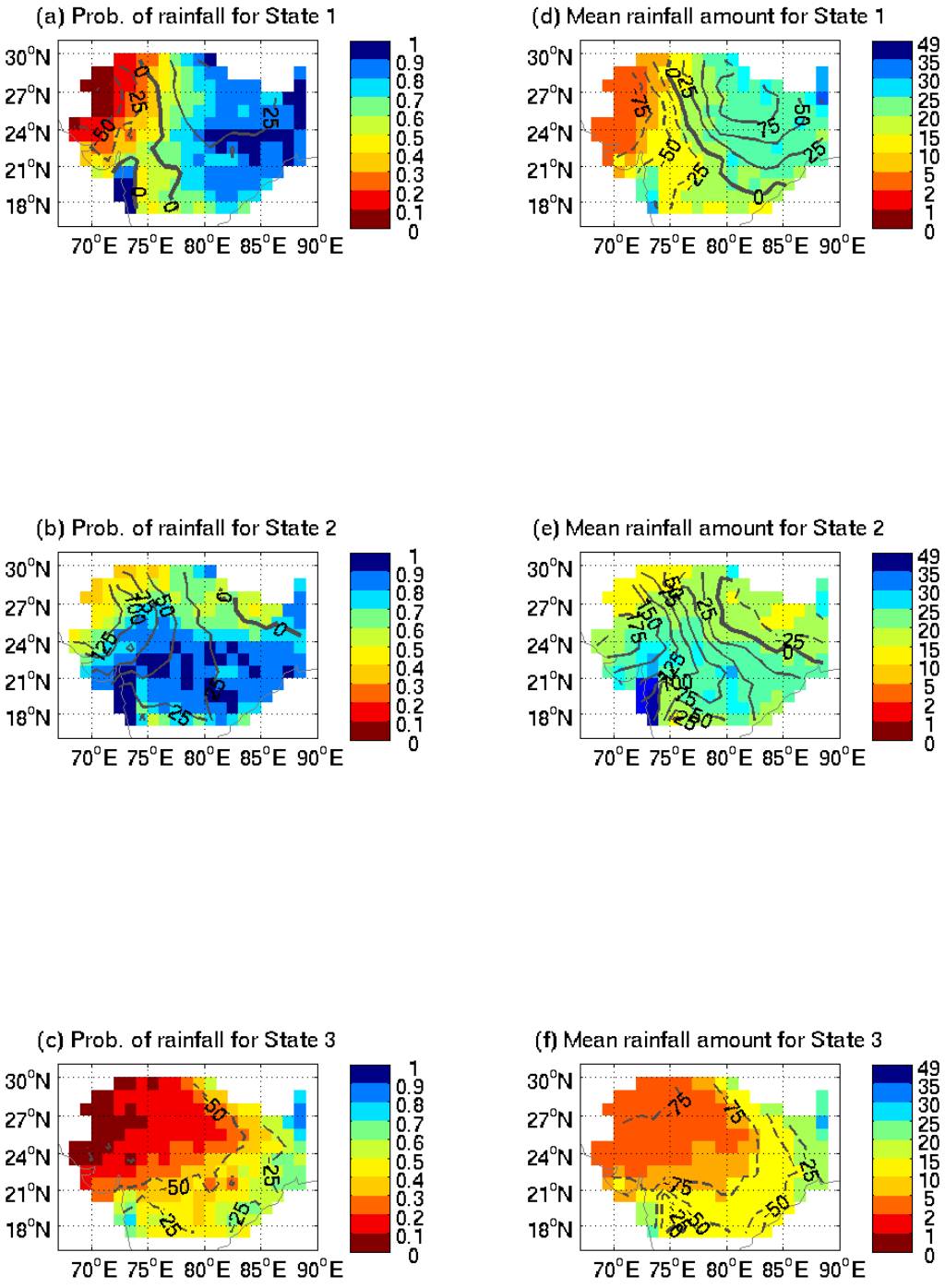
(a) Prob. of rainfall for State 1
(d) Mean rainfall amount for State 1
(b) Prob. of rainfall for State 2
(e) Mean rainfall amount for State 2
(c) Prob. of rainfall for State 3
(f) Mean rainfall amount for State 3
30°N
27°N
24°N
21°N
18°N
70°E 75°E 80°E 85°E 90°E
1 0.9 0.8 0.7 0.6 0.5 0.4 0.3 0.2 0.1 0
49 35 30 25 20 15 10 5 2 1 0

FIGURE 7

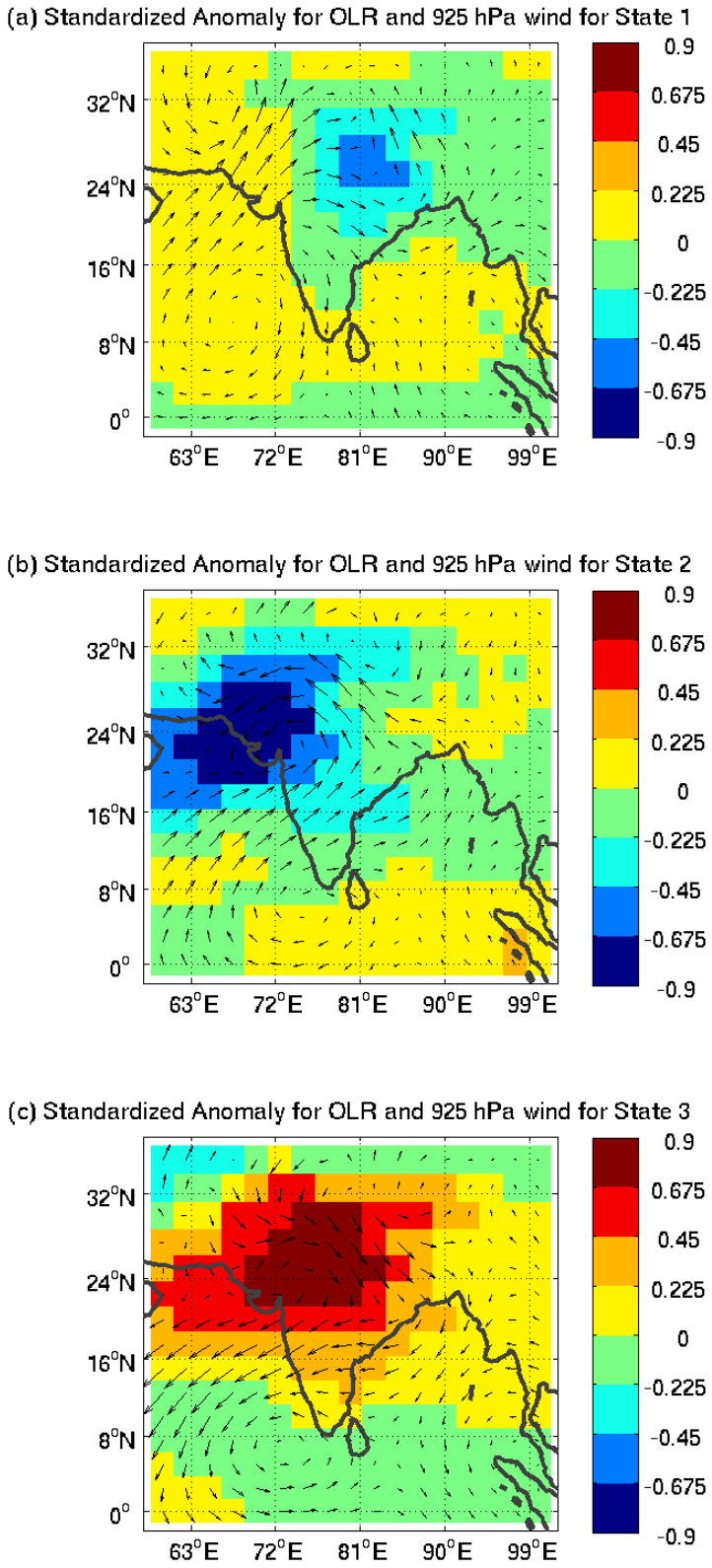
(a) Standardized Anomaly for OLR and 925 hPa wind for State 1
32°N
24°N
16°N
8°N
0°
63°E
72°E
81°E
90°E
99°E
0.9
0.675
0.45
0.225
0
-0.225
-0.45
-0.675
-0.9
(b) Standardized Anomaly for OLR and 925 hPa wind for State 2
32°N
24°N
16°N
8°N
0°
63°E
72°E
81°E
90°E
99°E
0.9
0.675
0.45
0.225
0
-0.225
-0.45
-0.675
-0.9
(c) Standardized Anomaly for OLR and 925 hPa wind for State 3
32°N
24°N
16°N
8°N
0°
63°E
72°E
81°E
90°E
99°E
0.9
0.675
0.45
0.225
0
-0.225
-0.45
-0.675
-0.9

FIGURE 8

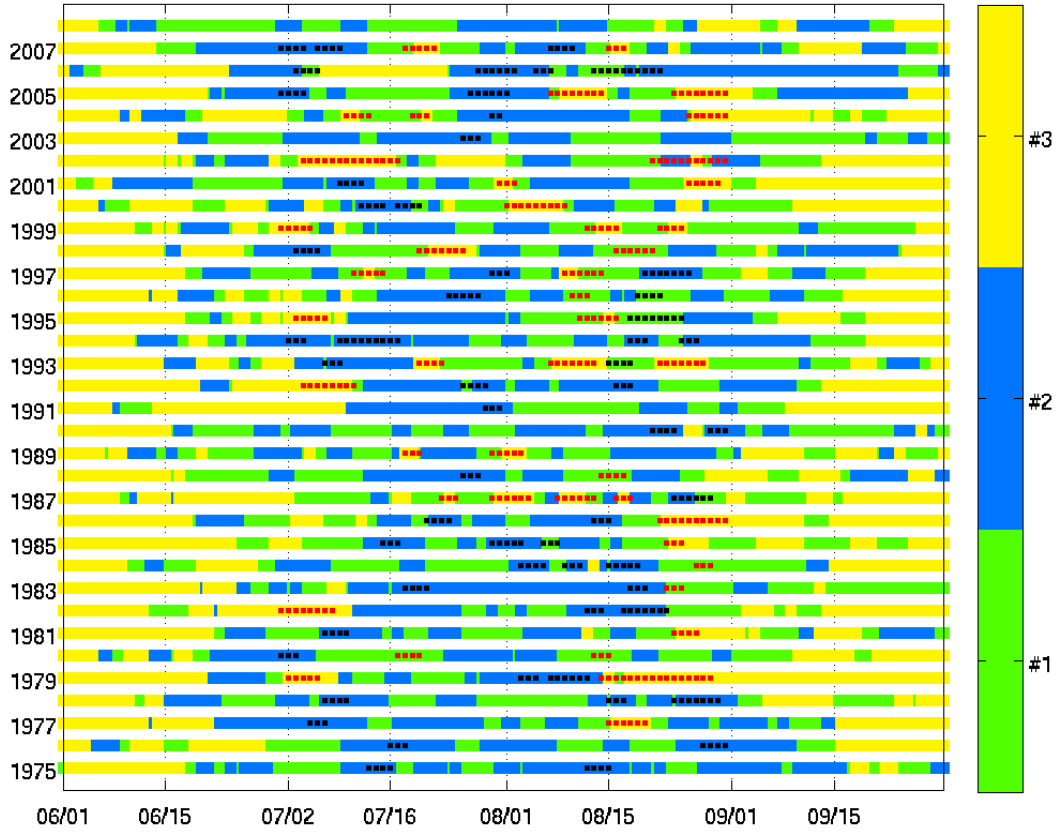
2007
2005
2003
2001
1999
1997
1995
1993
1991
1989
1987
1985
1983
1981
1979
1977
1975
06/01
06/15
07/02
07/16
08/01
08/15
09/01
09/15
#3
#2
#1

FIGURE 9

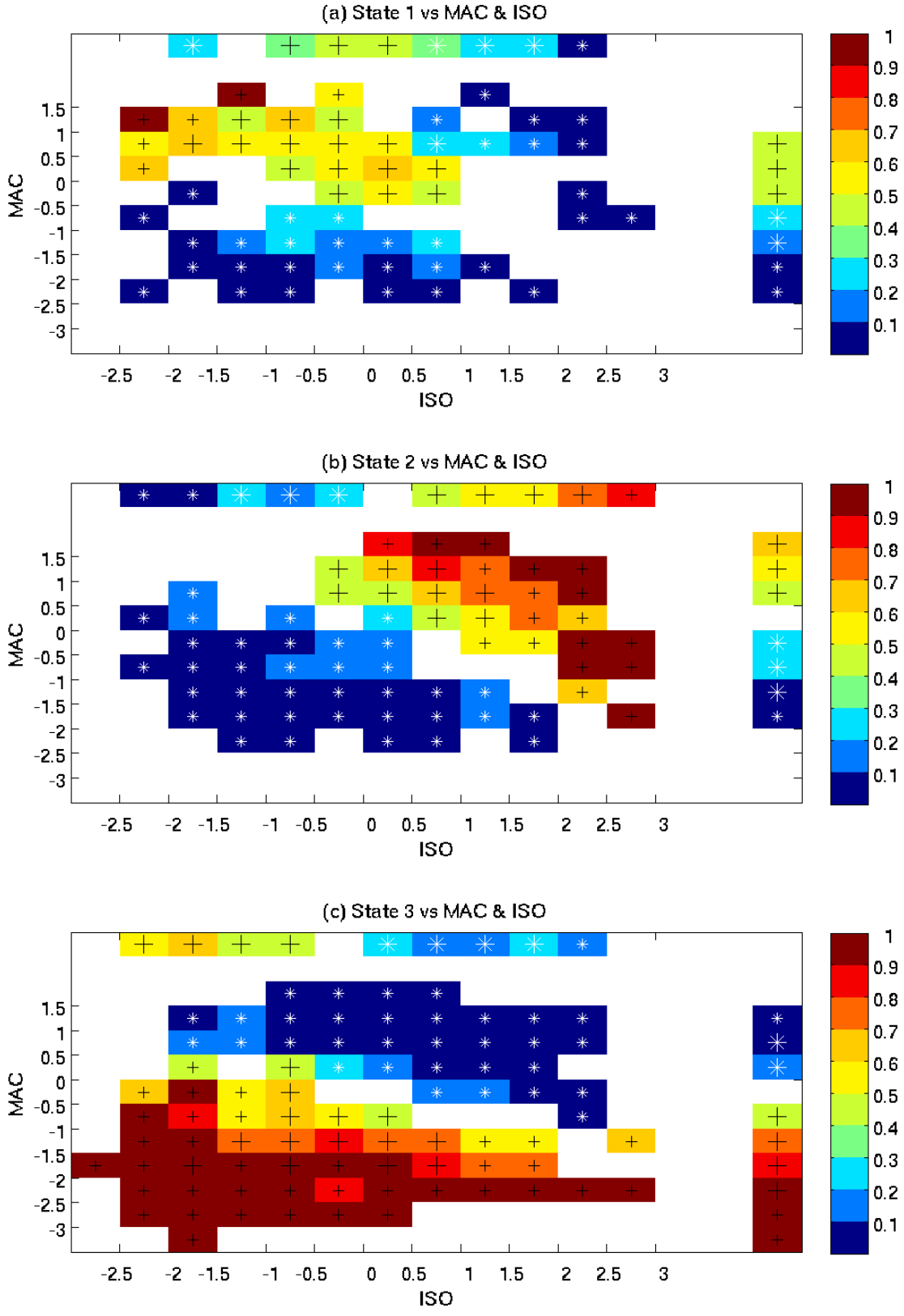
(a) State 1 vs MAC & ISO
(b) State 2 vs MAC & ISO
(c) State 3 vs MAC & ISO
MAC
ISO
1.5
1
0.5
0
-0.5
-1
-1.5
-2
-2.5
-3
-2.5
-2
-1.5
-1
-0.5
0
0.5
1
1.5
2
2.5
3
1
0.9
0.8
0.7
0.6
0.5
0.4
0.3
0.2
0.1

FIGURE 10

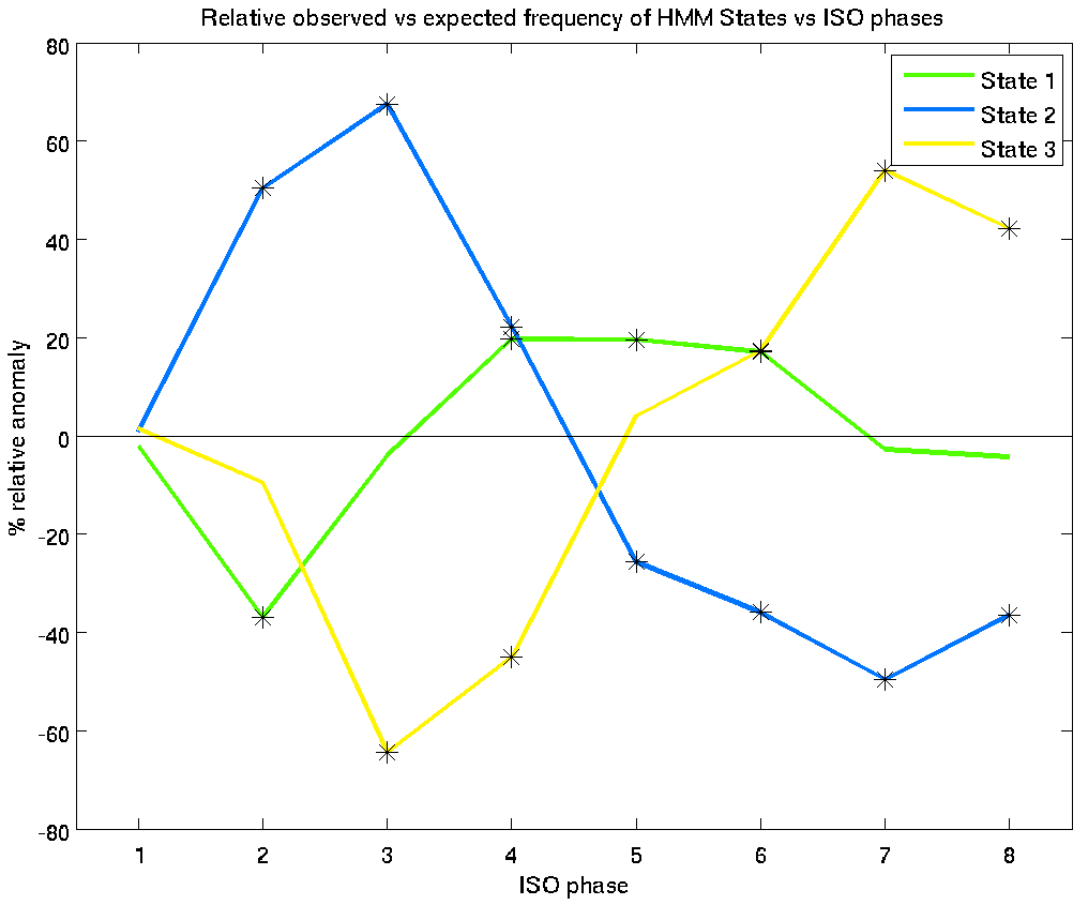
Relative observed vs expected frequency of HMM States vs ISO phases
State 1
State 2
State 3
% relative anomaly
ISO phase
80
60
40
20
0
-20
-40
-60
-80
1
2
3
4
5
6
7
8

FIGURE 11

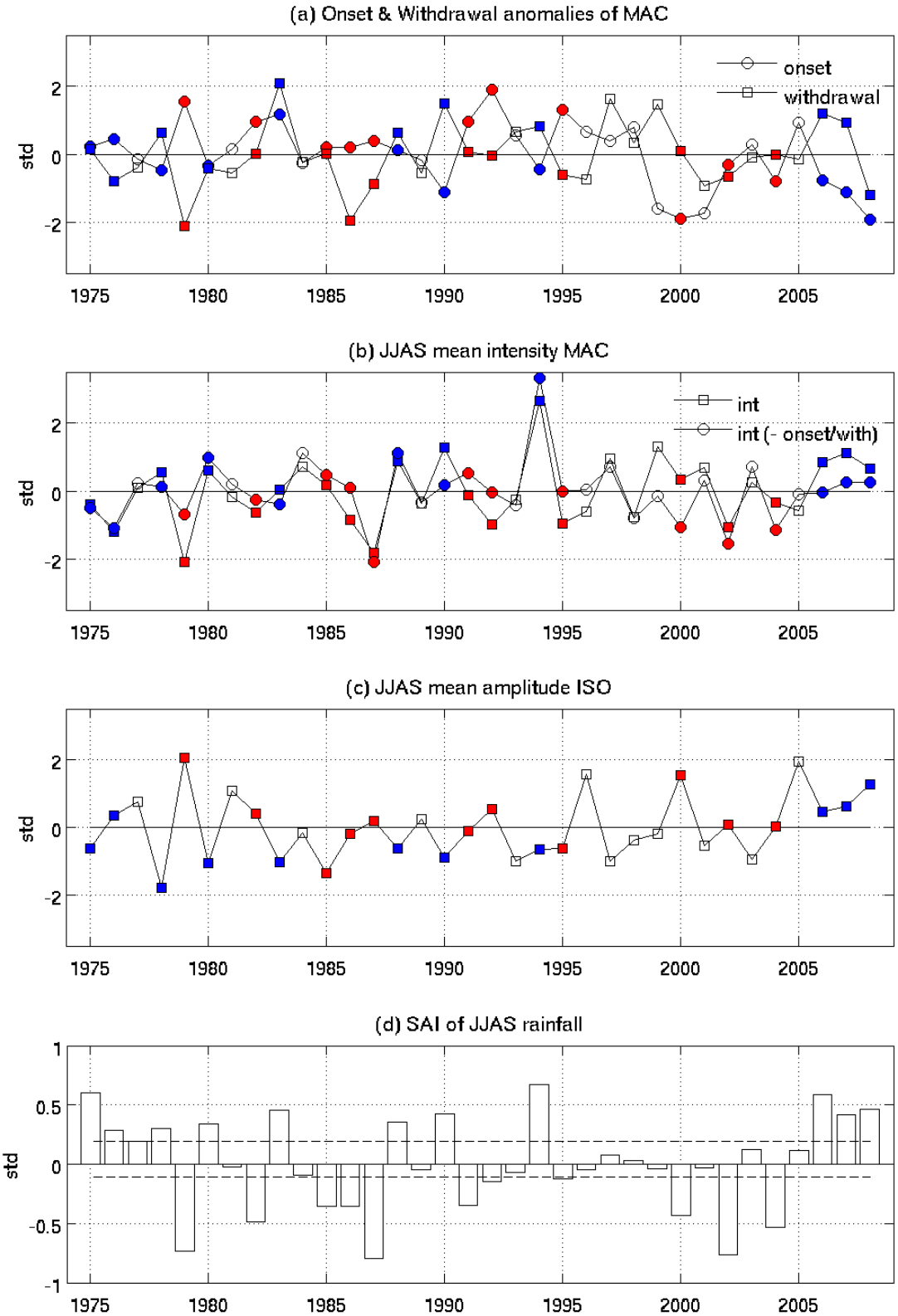
(a) Onset & Withdrawal anomalies of MAC
onset
withdrawal
std
2
0
-2
1975
1980
1985
1990
1995
2000
2005
(b) JJAS mean intensity MAC
int
int (- onset/with)
std
2
0
-2
1975
1980
1985
1990
1995
2000
2005
(c) JJAS mean amplitude ISO
std
2
0
-2
1975
1980
1985
1990
1995
2000
2005
(d) SAI of JJAS rainfall
std
1
0.5
0
-0.5
-1
1975
1980
1985
1990
1995
2000
2005

FIGURE 12

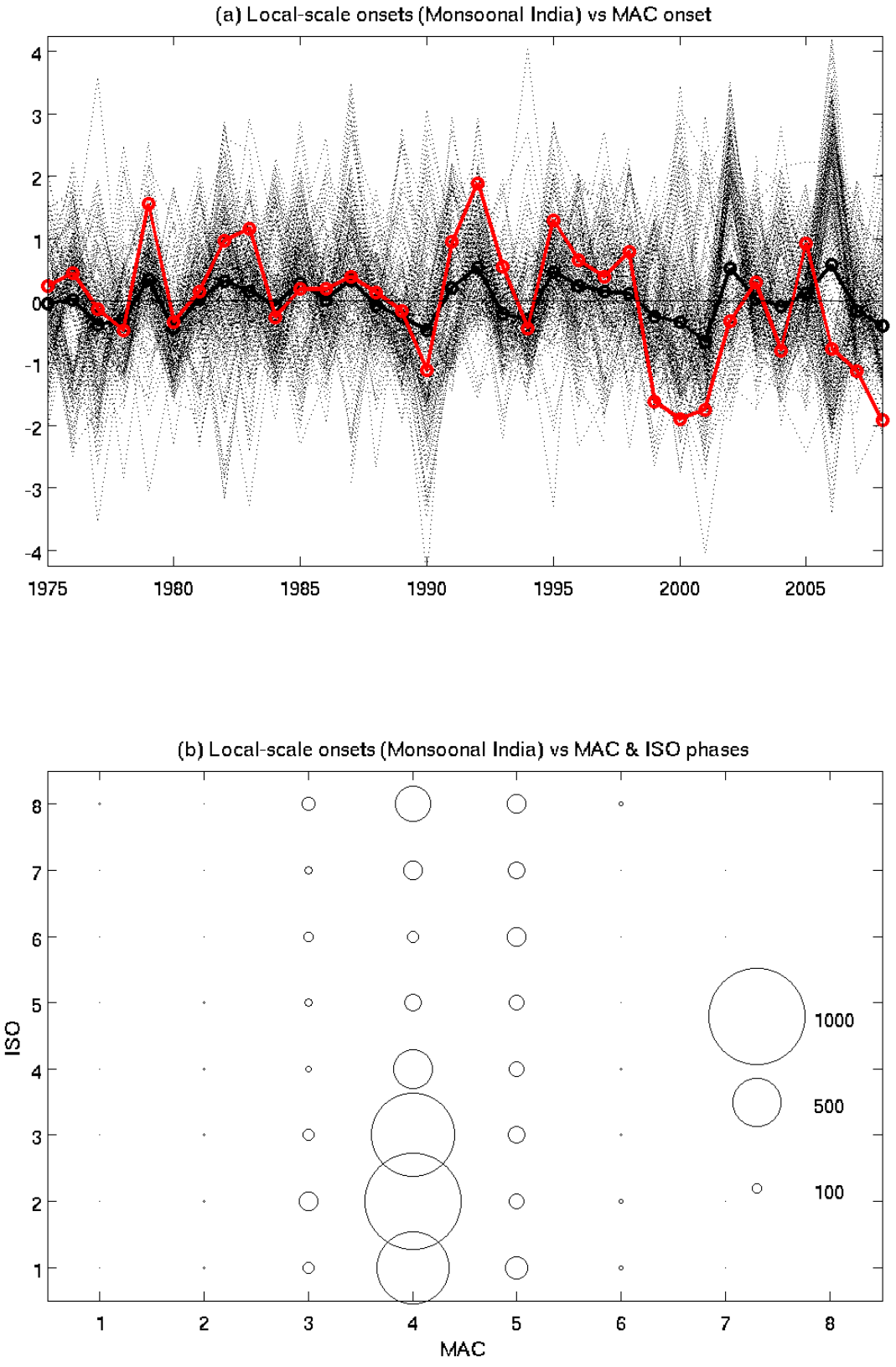
(a) Local-scale onsets (Monsoonal India) vs MAC onset
4
3
2
1
0
-1
-2
-3
-4
1975
1980
1985
1990
1995
2000
2005
(b) Local-scale onsets (Monsoonal India) vs MAC & ISO phases
ISO
MAC
1
2
3
4
5
6
7
8
1000
500
100

FIGURE 13

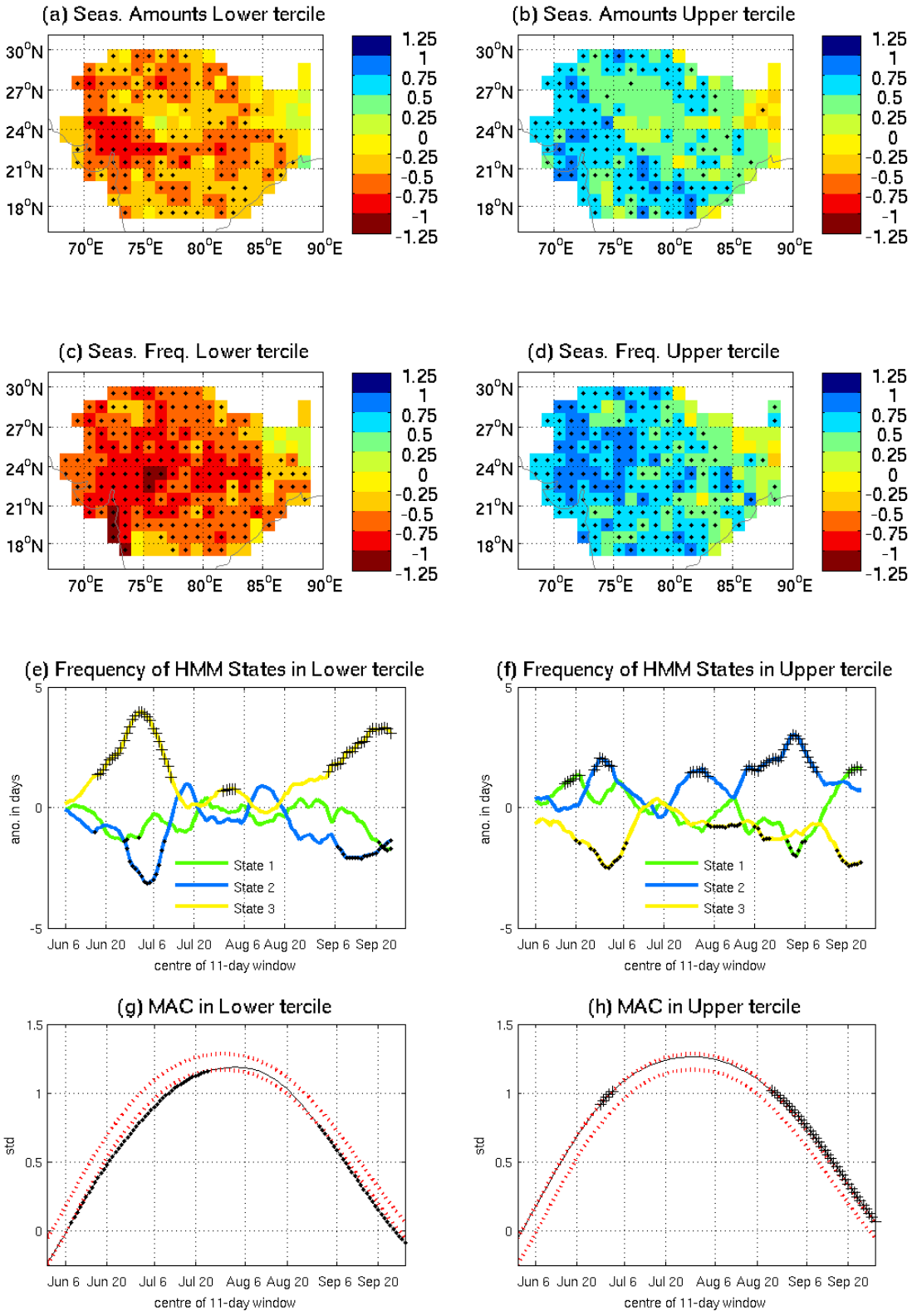
(a) Seas. Amounts Lower tercile
(b) Seas. Amounts Upper tercile
(c) Seas. Freq. Lower tercile
(d) Seas. Freq. Upper tercile
30°N
27°N
24°N
21°N
18°N
70°E 75°E 80°E 85°E 90°E
1.25 1 0.75 0.5 0.25 0 -0.25 -0.5 -0.75 -1 -1.25
(e) Frequency of HMM States in Lower tercile
(f) Frequency of HMM States in Upper tercile
ano. in days
State 1
State 2
State 3
Jun 6 Jun 20 Jul 6 Jul 20 Aug 6 Aug 20 Sep 6 Sep 20
centre of 11-day window
(g) MAC in Lower tercile
(h) MAC in Upper tercile
std

FIGURE 14

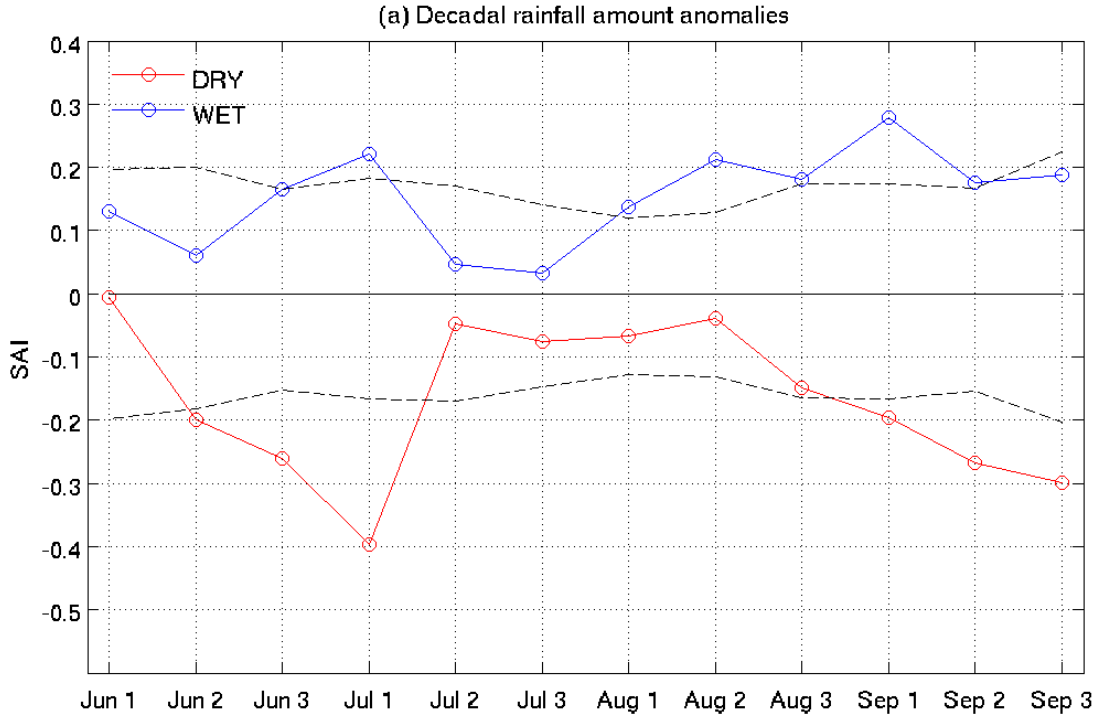
(a) Decadal rainfall amount anomalies
DRY
WET
SAI
0.4
0.3
0.2
0.1
0
-0.1
-0.2
-0.3
-0.4
-0.5
Jun 1
Jun 2
Jun 3
Jul 1
Jul 2
Jul 3
Aug 1
Aug 2
Aug 3
Sep 1
Sep 2
Sep 3

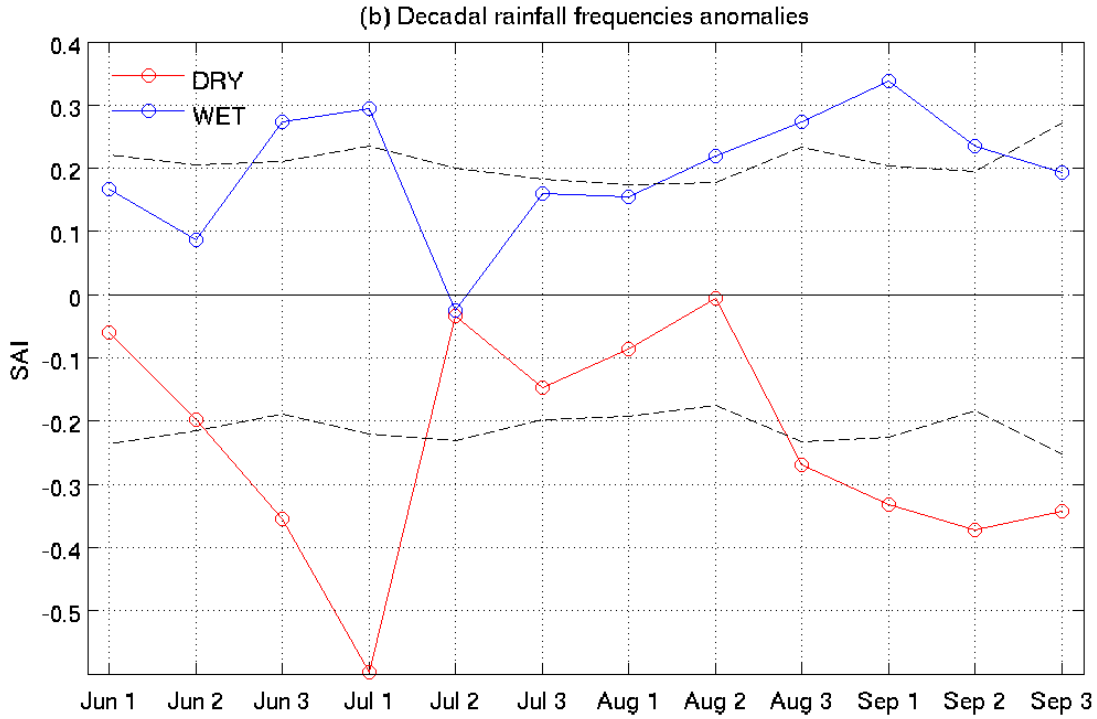
(b) Decadal rainfall frequencies anomalies
DRY
WET
SAI
0.4
0.3
0.2
0.1
0
-0.1
-0.2
-0.3
-0.4
-0.5
Jun 1
Jun 2
Jun 3
Jul 1
Jul 2
Jul 3
Aug 1
Aug 2
Aug 3
Sep 1
Sep 2
Sep 3

FIGURE 15